LAWRENCE
LIVERMORE
NATIONAL
LABORATORY

UCRL-JRNL-209600

Climate Change in Lowland Central America During the Late Deglacial and Early Holocene

M. B. Hillesheim, D. A. Hodell, B. W. Leyden, M. Brenner, J. H. Curtis, F. S. Anselmetti, D. Ariztegui, D. G. Buck, T. P. Guilderson, M. F. Rosenmeier, D. W. Schnurrenberger

February 10, 2005

Journal of Quaternary Sciences

Climate Change in Lowland Central America During the Late Deglacial and Early Holocene

Michael B. Hillesheim[1]*, David A. Hodell[1], Barbara W. Leyden[2], Mark Brenner[1], Jason H. Curtis[1], Flavio S. Anselmetti[3], Daniel Ariztegui[4], David G. Buck[5], Thomas P. Guilderson[6], Michael F. Rosenmeier[1,7], Douglas W. Schnurrenberger[8]

[1] Department of Geological Sciences and Land Use and Environmental Change Institute (LUECI), University of Florida, Gainesville, FL 32611, USA

[2] Department of Geology, University of South Florida, Tampa, FL 33620, USA

[3] Geological Institute, Swiss Federal Institute of Technology ETH, Zürich, Switzerland

[4] Institut Forel and Department of Geology, University of Geneva, Geneva, Switzerland

[5] School of Natural Resources and Environment and Land Use and Environmental Change Institute (LUECI), University of Florida, Gainesville, FL 32611, USA

[6] Center for Accelerator Mass Spectrometry, Lawrence Livermore National Laboratory, Livermore, CA 94551, USA

[7] Department of Geology and Planetary Science, University of Pittsburgh, Pittsburgh, PA 15260, USA (current address)

[8] National Lacustrine Core Repository and Limnological Research Center, University of Minnesota, Minneapolis, MN 55455, USA

*corresponding author (mbhilles@ufl.edu)

Submitted to Journal of Quaternary Science on 10 August 2004

Word Count: ~7,000

Key Words: Central America, Neotropics, paleoclimate, lake sediments, geochemistry, stable isotopes, pollen, Holocene, Preboreal, deglaciation, Intertropical Convergence Zone, 8.2-kyr Event

Abstract

The transition from arid glacial to moist early Holocene conditions represented a profound change in northern lowland Neotropical climate. Here we report a detailed record of changes in moisture availability during the latter part of this transition (~11,250 to 7,500 cal yr BP) inferred from sediment cores retrieved in Lake Petén Itzá, northern Guatemala. Pollen assemblages demonstrate that a mesic forest had been largely established by ~11,250 cal yr BP, but sediment properties indicate that lake level was more than 35 m below modern stage. From 11,250 to 10,350 cal yr BP, during the Preboreal period, lithologic changes in sediments from deep-water cores (>50 m below modern water level) indicate several wet-dry cycles that suggest distinct changes in effective moisture. Four dry events (designated PBE1-4) occurred at 11,200, 10,900, 10,700, and 10,400 cal yr BP and correlate with similar variability observed in the Cariaco Basin titanium record and glacial meltwater pulses into the Gulf of Mexico. After 10,350 cal yr BP, multiple sediment proxies suggest a shift to a more persistently moist early Holocene climate. Comparison of results from Lake Petén Itzá with other records from the circum-Caribbean demonstrates a coherent climate response during the entire span of our record. Furthermore, lowland Neotropical climate during the late deglacial and early Holocene period appears to be tightly linked to climate change in the high-latitude North Atlantic. We speculate that the observed changes in lowland Neotropical precipitation were related to the intensity of the annual cycle and associated displacements in the mean latitudinal position of the Intertropical Convergence Zone and Azores-Bermuda high-pressure system. This mechanism operated on millennial-to-submillennial timescales and may have responded to changes in solar radiation, glacial meltwater, North Atlantic sea ice, and the Atlantic meridional overturning circulation (MOC).

Introduction

The northern lowland Neotropics encompasses the area of the New World with elevations <500 m and extends north from the equator to the Tropic of Cancer. It includes areas of southern Mexico, Central America, and northern South America, as well as the West Indies (Fig. 1A). During the last deglaciation, this region experienced a pronounced increase in moisture availability. At the onset of deglaciation, all shallow lakes were dry and only deep basins contained water. The Petén Lake District of northern Guatemala (Fig. 1B) is one of the few regions with basins deep enough to have retained water during the arid late Pleistocene (Deevey *et al*., 1980). Cores recovered from Lakes Quexil (z_{max} = 32 m) and Salpetén (z_{max} = 32 m) in 1980 provided some of the first insights into climatic and ecological change in the lowland Neotropics during the last Ice Age and the transition to the Holocene (Deevey *et al*., 1983). Pollen and geochemical profiles demonstrated an abrupt shift from cool, arid conditions during the last glaciation to warmer, moister conditions during the early Holocene (Leyden *et al*., 1993, 1994; Brenner, 1994). Because of incomplete recovery, drilling disturbance, and poor dating resolution of the 1980 cores, details of the timing, rate and structure of this transition were uncertain.

In 1999, we completed a seismic survey (3.5 kHz) of six Petén lakes to identify potential targets for coring and drilling. We produced the first detailed bathymetric map of Lake Petén Itzá (Fig. 1C), the largest (100 km^2) and deepest (z_{max} = 160 m) lake in the region. Seismic profiles revealed a paleoshoreline feature at ~58 m below modern lake level that possibly represents the lake low-stand during the last glacial period (Anselmetti *et al*., in review). Because of the great depth of its northern basin, Lake Petén Itzá likely contains one of the few continuous sediment records in Central America of the last glaciation. Consequently, it is a

prime target for future drilling operations to obtain long, undisturbed sediment cores for paleoclimate studies.

In June 2002, we retrieved thirteen Kullenberg-type piston cores from 10 sites in Petén Itzá's northern basin (Fig. 1C). Undisturbed glacial-age sediment was not recovered because of the thickness of cohesive late Holocene sediments, which limited penetration of the piston corer to ≤6 m. The oldest continuous sediment record recovered is dated to 11,250 cal yr BP, and captures only the terminal part of the last deglaciation. Here we report on the paleoclimatic history of the Petén lowlands during the late deglacial and early Holocene period (~11,250 to 7,500 cal yr BP). We compare our results from Lake Petén Itzá with proxy records from other sites under the same climate regime, such as the marine Cariaco Basin off Venezuela (Haug *et al*., 2001), as well as with the climate history of the high-latitude North Atlantic recorded in marine sediments and Greenland ice cores (Bond *et al*., 2001; Stuiver *et al*., 1995). We find a coherent response of climate throughout the circum-Caribbean region during the late deglaciation and early Holocene with tight linkages to climate changes observed in the high-latitude North Atlantic.

Study Site

Lake Petén Itzá is located at ~17.00ºN, 89.50ºW in the Department of Petén, northern Guatemala (Fig. 1B). The lake is comprised of two connected basins. The deeper, northern basin (Z_{max} = 160 m) occupies a large half-graben formed by a series of east-west aligned *en echelon* faults (Vinson, 1962). The northern shore is marked by a steep karst ridge consisting of lower Tertiary limestone that follows the strike of the fault system, whereas the southern shore is

gently sloping and, in places, rimmed by poorly drained seasonal swamps (*bajos*). The smaller southern basin is much shallower, averaging ~5 m water depth.

Lake Petén Itzá's water is dilute (11.22 meq l^{-1}) and dominated by calcium and bicarbonate, with magnesium and sulfate following closely in concentration (Table 1). Lakewater pH is high (~8.0) and is saturated for calcium carbonate, and there are abundant shells of carbonate microfossils in the lake sediments (Covich, 1976; Curtis *et al*., 1998). Lake Petén Itzá is a terminal basin fed by precipitation, subsurface groundwater inflow, and a small input stream in the southeast. The basin is effectively closed, lacking any surface outlets, although some downward leakage may occur. The oxygen isotopic composition of lakewater averages 2.9‰, which is enriched by ~7‰ relative to regional groundwater (Table 1). This reflects the importance of evaporation on the lake's water budget. Thermal stratification is persistent year round with hypolimnetic temperatures averaging ~25.4ºC, close to the mean annual air temperature (Fig. 2A). Hypolimnetic oxygen depletion has been observed near the deepest point in the lake (Fig. 2B).

Petén's climate is marked by uniformly high temperatures (averaging 25ºC), and variability is most notably expressed by temporal and spatial changes in rainfall. Precipitation in Petén varies from 900 to 2500 mm yr^{-1}, with a regional mean of ~1600 mm yr^{-1} (Deevey *et al*., 1980). Lake Petén Itzá is situated in a climatically sensitive region where the amount of rainfall is related to the seasonal migration of the Intertropical Convergence Zone (ITCZ) and Azores-Bermuda high-pressure system (Hastenrath, 1984). Approximately 90% of the precipitation falls during the summer months (June to October) driven by increased convection associated with the northward migration of the ITCZ. The rainy season is often interrupted by a slight rainfall decrease in July and August, which is known as the canicula or "little dry" (Magaña *et al*.,

1999). The rainy season usually ends by late October and is followed by a pronounced dry season during the winter (January to May) as the ITCZ moves equatorward (i.e. southward), allowing the Azores-Bermuda high to dominate the Gulf of Mexico and Caribbean Sea region. The region is also marked by subsidence during winter related to the descending limb of the Hadley Cell, centered at ~20ºN (Waliser *et al*., 1999).

Lake Petén Itzá's volume is sensitive to precipitation changes and has fluctuated markedly in the recent past. For example, mean annual rainfall during the period from 1934 to 1942 was relatively high (2055 mm yr^{-1}) and resulted in increased lake levels and flooding (Deevey *et al*., 1980). In contrast, the early to mid-1970s were relatively dry (mean annual rainfall = 1415 mm yr^{-1}) resulting in lower lake levels. During the late 1970s lake level rose again in response to increased precipitation continuing until the early 1990s at which time the trend reversed. Petén Itzá's level varies seasonally, by as much as ~80 cm, displaying a rise after the summer rainy season and a fall during the dry season with a 1-2 month lag (Deevey *et al*., 1980). On seasonal to decadal time scales, lake volume and water chemistry are sensitive to changes in the balance between precipitation and evaporation.

Methods

In June 2002, we obtained six piston cores (Table 2) along a depth transect on seismic line 11 in water depths ranging from 9.7 to 63.2 m (Fig. 3). Cores were recovered using a Kullenberg-type piston corer triggered by a mud-water interface (MUCK) corer. In the laboratory, each core section was measured in its original polycarbonate liner for magnetic susceptibility and gamma-ray attenuation (GRA) bulk density at 0.5-cm increments using a GEOTEK Multi-Sensor Core Logger (MSCL). The instrument was calibrated at the start of each

day using an aluminum standard. After logging, cores were split and imaged with a GEOTEK digital color line-scan camera that was calibrated each day using a white ceramic calibration tile.

The primary focus of this study is on deep-water cores PI 8-VI-02 11A (water depth = 58.2 m), PI 5-VI-02 11B (water depth = 51.6 m), and shallow-water Core PI 6-VI-02 11D (water depth = 20.9 m); hereafter referred to as Cores 11A, 11B, and 11D. Core 11B was converted to the same sediment depth scale as Core 11A by correlating variations in color (rgb) intensity (correlation coefficient, r = 0.84) using Analyseries 1.1 (Paillard *et al*., 1996). The working halves of Cores 11A and 11B were sampled at 1-cm and 5-cm intervals, respectively. Small subsamples (~5 cc) were taken for elemental analysis, oven dried, and ground to a fine powder with a mortar and pestle. The remainder of the sample was wet sieved at 63-μm to isolate microfossils and terrestrial organic material for isotopic and radiocarbon analysis. The three shallow-water cores are PI 9-VI-02 11C, PI 6-VI-02 11D, and PI 8-VI-02 11E (Table 2). Core 11D was selected as representative of the sediment stratigraphy in shallow-water cores (<35 m water depth) and was sampled at 5-cm intervals for elemental composition and pollen analysis.

Radiocarbon ages were determined at the Center for Accelerator Mass Spectrometry (CAMS) at Lawrence Livermore National Laboratory. Eighteen samples of terrestrial organic matter (wood, leaf, or charcoal) and eight samples of aquatic gastropod (*Pyrgophorus* sp.) shell were dated. Samples of shell material were used to date intervals where terrestrial organic matter was scarce. Samples of terrestrial organic matter used for radiocarbon dating were pretreated at the University of Florida using the acid-base-acid pretreatment method. Radiocarbon ages were determined after blank subtraction as determined on similarly pretreated and processed ^{14}C-free wood. Organic matter samples were also analyzed for δ^{13}C content and corrected to –25‰ prior to calibration. Five samples from Core 11A were too small for δ^{13}C analysis and were assumed

to have values of –25‰. Calibrated ages, in calendar years before 1950 (cal yr BP), were calculated using INTCAL98, with a 100-yr moving average of the tree ring calibration data set (Stuiver and Reimer, 1993; Stuiver *et al*., 1998).

Inorganic carbon (IC) was determined by coulometric titration using a UIC/Coulometrics 5011 coulometer coupled with a UIC 5240-TIC carbonate autosampler. Weight percent calcium carbonate ($CaCO_3$, %) was calculated by multiplying IC by 8.33. Total weight percent carbon (TC) and sulfur (S, %) were measured using a Carlo Erba NA 1500 CNS elemental analyzer with autosampler. Weight percent organic carbon (OC) was estimated by subtracting IC from TC. Weight percent organic matter (OM, %) was estimated by multiplying OC by 2.2.

Oxygen isotope ratios in Core 11A were measured on adult carapaces of the ostracod *Limnocythere* sp., which were isolated from the >250 μm sediment fraction. Ostracod valves were abundant from 558 to 500 cm, but gradually decreased above this level until they became absent at 484 cm. Ostracods were cleaned with 15% H_2O_2 to remove organic matter, and then washed with de-ionized water, rinsed in methanol, and dried. Ostracod aggregates of 15-20 valves were measured from each 1-cm sample. The samples were reacted in 100% orthophosphoric acid at 70ºC using a ThermoFinnigan Kiel III automated preparation system. Isotopic ratios of purified CO_2 gas were measured online with a ThermoFinnigan 252 mass spectrometer. All isotopic values are reported in standard delta (δ) notation relative to the VPDB standard. Analytical precision was estimated by measuring eight samples of a powdered carbonate standard (NBS-19) with each sample run. Precision for $\delta^{18}O$ was estimated to be ±0.10‰ (1σ; n = 24 standards).

Samples for pollen analysis were processed using 1-cm^3 of sediment taken from Core 11B at 1-cm to 10-cm intervals and Core 11D at 5-cm intervals. One *Lycopodium* tablet (batch

124961; mean = 12,542; std. dev. = ± 931) was added to each sample to calculate pollen concentration. Samples were processed using a standard sequence of HCL, KOH, HF, and acetolysis. The residue was stained with Basic Fuchsin and suspended in tertiary butyl alcohol (TBA), and measured aliquots of the suspension were mounted in silicone oil on microscope slides. Pollen from Core 11D were counted at 400x magnification to a minimum sum of 200, excluding pteridophytes, aquatic algae and macrophytes, and unidentifiable grains. For Core 11B, *Brosimum*-type pollen was also excluded from the sum to enhance the representation of the other taxa. Concentrations were converted to accumulation rates (grains cm^{-1} yr^{-1}) using the age model for Core 11B.

Results

Radiocarbon

All thirteen radiocarbon samples from Core 11A yielded dates in stratigraphic order (Table 3). An age-depth model was derived by linear interpolation between dated horizons (Fig. 4). We estimated the basal age of Core 11A to be ~11,250 cal yr BP by extrapolating the linear sedimentation rate 6 cm beyond the lowermost radiocarbon date at 552 cm. Linear sedimentation rates (Fig. 4) average ~0.025 cm yr^{-1} from the base of the core at 558 cm to 335 cm (11,250 to 3,000 cal yr BP). Between 335 and 57 cm (3,000 to ~1,400 cal yr BP), sedimentation rates increase to ~0.2 cm yr^{-1}. The temporal resolution averages ~40 yrs for each 1-cm sample during the late deglacial and early Holocene part of the sequence (558 to 463 cm or 11,250 to 7,500 cal yr BP). Charcoal near the top of a soil horizon found in the three shallow-water cores (Table 3; Fig. 3B) was dated to constrain the onset of lacustrine deposition (i.e. flooding surface) associated with lake filling. Ages ranged from 11,120 ± 60 cal yr BP in Core

11C (31.8 m water depth) to 10,220 ± 70 cal yr BP in Core 11E (9.7 m water depth). In addition, three shell samples from the base of each shallow-water core were dated, yielding ages between 20,540 and 37,650 cal yr BP (Table 3; Figure 3B).

Lithology and Geochemistry

Shallow-water cores: Sediment properties of Core 11D (Fig. 5) represent the general pattern of lithologic and geochemical changes observed in the three shallow-water cores (<35 m water depth). Pleistocene age sediments consist of dense, carbonate-rich silty-clays overlain by a paleosol that is marked by increased magnetic susceptibility (Fig. 5D), the presence of terrestrial gastropods and plant roots, and the absence of aquatic microfossils. The transition to lacustrine deposition, dated between 11,100 and 10,200 cal yr BP (Fig. 3B), is marked by decreases in density and magnetic susceptibility concurrent with increases in percent carbonate and organic matter content (Fig. 5), as well as the reappearance of lacustrine gastropods and ostracods.

Deep-water cores: The bottom 25 cm (~11,250 to 10,350 cal yr BP) in both deep-water cores (11A, 11B) is composed of dense gypsum sands interbedded with silty clays. These lithologic changes are reflected in the calcium carbonate ($CaCO_3$), organic matter (OM), and sulfur (S) records (%, Fig. 6A-C). Gypsum-rich intervals are indicated by high sulfur content centered at ~10,400, 10,700, 10,900, and 11,200 cal yr BP. The intervening silty-clay layers contain higher percentages of carbonate and organic matter and are centered at ~10,500, 10,800, and 11,000 cal yr BP. At 10,350 cal yr BP, gypsum precipitation ceased and sediments became dominated by calcium carbonate and organic matter. Between 10,350 and 7,500 cal yr BP, $\%CaCO_3$ decreased from 60 to 10% and %OM increased slightly, averaging 14%, with the remainder of the sediment being composed mostly of inorganic clay. Superimposed upon these long-term trends are small, short-term variations. At 9,700 cal yr BP, $\%CaCO_3$ decreased by

25% and %OM increased by ~10%. From 9,700 to 8,800 cal yr BP, $\%CaCO_3$ and %OM remained relatively constant averaging 25 and 14%, respectively. At 8,800 cal yr BP, $\%CaCO_3$ began to decrease more rapidly coincident with a distinct increase in %OM. This trend is interrupted at 8,100 cal yr BP by a ~10% decrease in organic matter and a ~5% increase in carbonate, relative to the bulk sediment, that persisted until 7,800 cal yr BP when both proxies returned to pre-excursion values.

GRA bulk density follows lithologic changes between 11,250 and 10,350 cal yr BP. High density is associated with gypsum beds and low density with clay-rich layers (Fig. 6D). At 10,350 cal yr BP, density decreased abruptly followed by progressively lower values until the end of the record at 7,500 cal yr BP. This trend was interrupted, however, by a small (0.1 g cc^{-1}), short-lived (~100 yr) increase centered at 9,400 cal yr BP and a larger (0.2 g cc^{-1}), longer-lived (~300 yr) increase centered at ~8,000 cal yr BP.

Ostracods from the base of Core 11A record the greatest $\delta^{18}O$ values averaging 4.5‰ (Fig. 6E). Between ~11,250 and 10,400 cal yr BP, $\delta^{18}O$ generally decreased by ~1.3‰. Superimposed upon this trend are two distinct $\delta^{18}O$ minima centered at 11,000 and 10,500 cal yr BP. At 10,400 cal yr BP, $\delta^{18}O$ values increased slightly and then gradually decreased until ~9,600 cal yr BP, at which point values begin to increase again. At 9,300 cal yr BP, this trend reversed and $\delta^{18}O$ reached its lowest values of ~3.1‰ at 8,800 cal yr BP. Ostracods are absent in the sediment profile after this time.

Pollen

Pollen is poorly preserved prior to ~11,500 cal yr BP (86 cm) in Core 11D (Fig. 7A). Within the soil horizon (75 to 115 cm), *Pinus* (pine) predominates together with *Quercus* (oak), Asteraceae (composites), and Poaceae (grasses), but pollen concentrations are low. A small

increase in aquatic taxa occurs as lacustrine deposition begins at 10,670 cal yr BP (75 cm). After which *Brosimum*-type becomes a dominant taxon, along with *Gymnanthes*, pine, oak, *Bursera*, and grasses.

The pollen percentage profile for Core 11B (Fig. 7B) can be divided into three zones that correlate with the sedimentological and isotopic records, but typically lag behind them by ~100 yrs based on the high-resolution sampling of pollen (i.e. 1-cm intervals) over the late deglacial-to-early Holocene transition. Total pollen accumulation rates in Core 11B were low prior to 10,250 cal yr BP, less than one-third of the values calculated for later deposits. Subsequent accumulation rates follow the percentage trends. *Brosimum*-type predominates in the basal zone from 11,250 to 10,250 cal yr BP together with *Bursera*, *Ulmus*, *Gymnanthes*, pine, and oak. Percentages for *Liquidambar* (sweet gum), *Typha* (cattail) and Asteraceae are notable. From 10,250 to 8,250 cal yr BP *Brosimum*-type, other Moraceae, *Celtis,* and Melastomataceae/ Combretaceae increase while *Liquidambar,* oak, and to a lesser extent, *Gymnanthes* decline. The aquatic alga *Botryococcus* increases sharply by 8,800 cal yr BP. After 8,300 cal yr BP *Brosimum*-type and *Gymnanthes* decrease and secondary forest taxa such as *Bursera* and *Cecropia* increase, followed later by increases in *Byrsonima*, grasses, and charcoal.

Interpretation of Proxies

The oxygen isotopic ($\delta^{18}O$) composition of shell carbonate is influenced by temperature, $\delta^{18}O$ of lake water, and vital effects (i.e. taxon-specific fractionation) (Covich and Stuiver, 1974). Vital effects were minimized by measuring a single species of adult ostracod (*Limnocythere* sp.) from the >250 μm sediment fraction. Temperature change in the region during the Preboreal and early Holocene was probably small given the minor change in pollen

assemblage relative to the last glacial, as well as the lack of cool indicator species such as *Juniperus* and *Liquidambar*. We therefore suggest that ostracod $\delta^{18}O$ was controlled principally by changes in the $\delta^{18}O$ of lake water, which is related to the ratio of evaporation to precipitation (E/P) and the $\delta^{18}O$ of precipitation (Fontes and Gonfiantini, 1967; Gasse *et al*., 1990). Between 11,500 and 8,700 cal yr BP, the $\delta^{18}O$ of western Caribbean seawater decreased by ~0.4‰ (Schmidt *et al*., 2004), which should have decreased the $\delta^{18}O$ of precipitation by the same amount because the Caribbean is the primary source of water vapor to the Yucatan Peninsula. The $\delta^{18}O$ of precipitation in the tropics is also dependent on the amount of rainfall, with lower $\delta^{18}O$ values associated with greater precipitation (Rozanski et al., 1993). Both the "amount effect" and changes in E/P influence lakewater $\delta^{18}O$ in the same direction such that increased precipitation results in lower $\delta^{18}O$ values of both rainfall and lake water. We conclude that variations in Lake Petén Itzá ostracod $\delta^{18}O$ represent relative changes in the ratio of precipitation to evaporation. Times of changing E/P are represented by changes in the slope of $\delta^{18}O$ and periods of unchanging $\delta^{18}O$ represent times of fairly constant E/P. We therefore compared the first derivative (i.e. changing slope) of the $\delta^{18}O$ signal with other proxy records (Fig. 8).

Changes in precipitation affect delivery rates of detrital material to the lake basin. Changing rainfall also alters the concentration of dissolved salts by enriching or diluting ions in lake water. We used sediment lithology and chemical composition to infer past changes in detrital input and lake water chemistry that are, in turn, controlled by climate. For example, greater gypsum content in sediments and associated increases in sediment density reflect lake volume reduction and higher lakewater salinity during dry periods, similar to the interpretation of the record from Lake Chichancanab, northern Yucatan Peninsula (Hodell *et al*., 1995, 2001, in press). Scanning electron micrographs (SEMs) of gypsum grains from Lake Petén Itzá show

they are euhedral and have no evidence of rounding or abrasion that would indicate transport or redeposition. We suggest that gypsum formed authigenically in the littoral zone where the evaporation rate is higher than that in deeper, open water.

Discussion

Paleoclimatic History of Lake Petén Itzá

Seismic profiles suggest that lake level was ~58 m below modern prior to 11,250 cal yr BP (Fig. 3A; Anselmetti *et al*., in review), which required an ~87% (4.8 km^3) reduction in volume relative to today (Fig. 9). Shallow-water cores (<35 m below modern lake level) contain a paleosol indicating subaerial exposure. Cores from nearby, shallower Lakes Quexil and Salpetén also indicated lake level lowering of at least 30-40 m during the last glacial period (Deevey *et al*., 1983), which likely caused them to become ephemeral. Glacial-age vegetation consisted of sparse temperate thorn scrub and taxa such as *Juniperus* indicating much cooler temperatures. One estimate suggests that temperatures were ~6.5 to 8ºC lower than today (Leyden *et al*., 1993, 1994).

During the last deglaciation, Petén climate was marked by an abrupt shift from arid to humid conditions, as inferred from multiple sediment proxies (Leyden *et al*., 1993, 1994; Brenner, 1994). Pollen assemblages in shallow-water Core 11D (Fig. 7A) changed from *Pinus* to *Brosimum*-type dominance concomitant with the rise of other mesic taxa. This increase in mesic taxa correlates with a similar change in the pollen profile from nearby Lake Quexil that occurred after ~12,600 cal yr BP (Leyden *et al*., 1993, 1994).

Deep-water cores from Lake Petén Itzá do not capture the entire deglacial sequence. Instead, they begin during the latter part of deglaciation, at ~11,250 cal yr BP. Predominance of

Brosimum at the base of Core 11B indicates a mesic tropical forest had largely been established in Petén by this time (Fig. 7B). This is in agreement with $\delta^{18}O$ and pollen records from Lake Quexil that indicate warmer and wetter conditions following the glacial period (Leyden *et al*., 1993, 1994). Dated paleosols in shallow-water Petén Itzá cores, however, indicate lake level was at least 35 m lower than today (Fig. 3B). This conclusion is supported by the presence of *Typha* pollen in deep-water cores (>50 m) that indicates a nearby littoral zone with emergent vegetation (Fig. 7B).

From 11,250 to 10,350 cal yr BP, during the Preboreal period, the $\delta^{18}O$ of Lake Petén Itzá ostracods in Core 11A decreased, indicating greater effective moisture (Fig. 6E). The lithologic change in shallow-water cores (<35 m water depth), from subaerial exposure (paleosol) to subaqueous deposition (lacustrine sediments), marks a lake level rise at this time (Figs. 3B and 5). In deep-water Core 11A, variations in oxygen isotopes, density, and sediment composition records (Fig. 6) show a number of abrupt changes that suggest varying effective moisture and lake level instability. These changes represent a series of wet-dry cycles of ~250 yr duration. During the Preboreal, four distinct dry events (designated PBE1-4) are identified by lithologic changes (i.e., increased gypsum content) centered at 11,200, 10,900, 10,700, and 10,400 cal yr BP (Fig. 8). Changes in $\delta^{18}O$, as expressed by the first derivative of the signal, are consistent with the lithologic changes, typically leading them by ~50 yrs (Figs. 8).

Low temporal sampling resolution (~50-200 yrs) for pollen over this interval precludes detailed interpretation of vegetation changes during this period. Average climate conditions at the beginning of the Preboreal were somewhat cooler and drier. But after ~10,700 cal yr BP, pine, oak, *Liquidambar*, and *Gymnanthes* begin to decline while *Acalypha, Trema,* and charcoal increase (Fig. 7B). *Liquidambar* reflects cooler conditions and *Gymnanthes* prefers drier, open

conditions. *Acalypha* and *Trema* are common tropical secondary or successional taxa. Although percentages for *Brosimum* don't increase, the accumulation rate is slightly higher. During this interval, pollen changes suggest moister, and perhaps warmer, climatic conditions, in general agreement with other proxy indicators.

An important change in Lake Petén Itzá's hydrology occurred at ~10,350 cal yr BP, coinciding with the Preboreal/Boreal boundary observed in northern European pollen records. At this time, an increase in effective moisture is inferred from sharp decreases in density and sulfur content that indicate cessation of gypsum precipitation (Fig. 6C,D) concomitant with increases in carbonate and organic matter content (Fig. 6A,B). A small increase in the abundance of *Brosimum*-type pollen lags this transition by ~100 yrs (Fig. 7B). This represents the time at which Lake Petén Itzá's water chemistry fell below gypsum saturation and sediment lithology and density became less variable.

After 10,350 cal yr BP, reduced variability of sediment composition and ostracod $\delta^{18}O$ values indicate a more persistent moist climate (Fig. 6). This is further supported by the resumption of lacustrine deposition at sites shallower than 8 m water depth (Fig. 3B; Curtis *et al*., 1998) indicating lake stage had risen to near present levels by 10,200 cal yr BP (Fig. 9). Centered at 9,400 cal yr BP, small increases in density and $\delta^{18}O$ may suggest a brief (~100 yr) return to slightly drier conditions (Fig. 6D,E). At 8,800 cal yr BP, the abundance of aquatic algae (*Botryococcus*) increases (Fig. 7B) concomitant with an increase in organic matter content (Fig. 6B). This also marks the time when ostracods in deep-water cores disappear, indicating the onset of hypolimnetic anoxia, which may also account for better preservation of organic matter. Between 8,100 and 7,800 cal yr BP, changes in sediment composition suggest a temporary return to drier conditions (Fig 6A-D), after which humid climate conditions prevailed again.

From 10,250 to 8,300 cal yr BP, the pollen record also indicates a relatively moist, stable climate. The continued prominence of *Gymnanthes*, however, suggests that parts of the watershed were still edaphically dry or unstable, perhaps on some of the steep basin slopes. Given the limited sampling resolution (~200 yr) over this interval, the pollen record suggests drier conditions between 8,100 and 7,800 cal yr BP, consistent with lithologic changes. This period also marks the beginning of fundamental changes in the vegetation, that include the introduction of other secondary taxa such as *Cecropia* that reflect a more diverse, open forest and increased seasonality (Fig. 7B).

Comparisons with other Circum-Caribbean and North Atlantic Records

Here we compare our results with other marine and lake records from the circum-Caribbean and Gulf of Mexico, in order to assess the regional extent of paleoclimatic changes observed in Lake Petén Itzá proxies. Previous studies of the last glacial-to-interglacial cycle have reported similarities between climate change in the Caribbean and the high-latitude North Atlantic on a variety of time scales (Hughen *et al*., 1996; Peterson *et al*., 2000). Consequently, we also compare the Petén Itzá record with proxy signals from the high latitudes of the Northern Hemisphere. When comparing Lake Petén Itzá proxies with other paleoclimate records, each signal was plotted on its own independent timescale and no attempt was made to align features in the records.

There are relatively few lacustrine records of the last deglaciation in the circum-Caribbean because most shallow lakes remained dry well into the early Holocene. Lake Miragoane, Haiti, and Lake Valencia, Venezuela, are two lakes located on the northern and southern rim of the Caribbean Basin, respectively, that were deep enough to preserve records of the latter part of the last deglaciation (Bradbury *et al*., 1981; Leyden, 1985; Hodell *et al*., 1991;

Curtis and Hodell, 1993; Brenner *et al*., 1994; Higuera-Gundy *et al*., 1999; Curtis *et al*., 1999, 2001). Between 11,250 and 8,800 cal yr BP, oxygen isotopic records from Lakes Miragoane, Valencia and Petén Itzá are similar, showing large-scale fluctuations superimposed on a long-term trend of increasing moisture availability (Fig. 10). Several $\delta^{18}O$ maxima and minima can be correlated among the records within the uncertainty of the chronologies. The records from Lakes Valencia and Petén Itzá are the most reliably dated because the chronologies are based exclusively on radiocarbon analysis of discrete terrestrial macrofossils. In contrast, the Lake Miragoane chronology is based on radiocarbon analysis of carbonate microfossils with the assumption of a constant hard-water lake error. Despite the dating uncertainty in Lake Miragoane the pattern of oxygen isotope variation is similar to those from the other lakes indicating several abrupt shifts in moisture availability on an otherwise long-term trend toward wetter conditions in the early Holocene.

The most detailed records of the last deglaciation and Holocene in the Caribbean come from studies of laminated sediments in the Cariaco Basin (11ºN) off the coast of Venezuela (Haug *et al*., 2001, Peterson *et al*., 2000, Hughen *et al*., 1996). In general, the density record from Lake Petén Itzá Core 11A and the titanium (Ti) record from Cariaco (Haug *et al*., 2001) are remarkably similar (Fig. 11). Both sediment proxies are probably related indirectly to precipitation. In Cariaco, rainfall controls the input of terrigenous material to the basin. Low Ti values in Cariaco sediments have been interpreted to reflect drier climate and vice-versa. In Lake Petén Itzá, detrital input and lake water chemistry control sediment composition, which is related indirectly to precipitation.

The Petén Itzá record does not extend back to the time of the Bølling-Allerød or Younger Dryas events that are prominent in the Cariaco Ti signal, but rather begins in the Preboreal

period when Cariaco Ti values were generally increasing but lower than those of the early Holocene. The late deglacial is marked by density variations in Core 11A that correspond to changes in Ti content of Cariaco Basin sediments. Within dating uncertainties, reductions in Cariaco Ti content correlate to intervals of increased density and gypsum content in Lake Petén Itzá (Fig. 11B), suggesting that the dry Preboreal events (PBE1-4) observed in the Petén Itzá record may have been pan-Caribbean in extent.

At the end of the Preboreal period (~10,350 cal yr BP), both records show an abrupt shift that suggests increased precipitation (Fig. 11A). This transition is more pronounced in the Petén Itzá density record than in Cariaco Ti owing to the sudden cessation of gypsum deposition in the lake. During the early-to-middle Holocene, the two records track one another closely, and display two synchronous returns to inferred drier conditions (Fig 11A). The first, centered at 9,400 cal yr BP was small and brief (~100 yrs). The second, centered at 8,000 cal yr BP, was greater in magnitude and longer in duration (~300 yrs). The latter event is also recoded in a speleothem from lowland Costa Rica, that suggests this was a time of protracted dry conditions associated with a weakening of the Central American monsoon (Lachniet *et al.*, 2004).

The Gulf of Mexico may have played an important role in regional climate during the last deglaciation because of meltwater input derived from the retreat of the Laurentide Ice Sheet. Many studies have focused on the early part of the last deglaciation (i.e. Bølling-Allerød/Younger-Dryas transition) when meltwater was redirected from the Mississippi River to the St. Lawrence River into the North Atlantic (Clark *et al.*, 2001). A recent study, however, suggests that episodic meltwater floods to the Gulf of Mexico continued after the Younger-Dryas period. Aharon (2003) identified four events during the Preboreal, when meltwater was rerouted south. These are centered at 9,900, 9,700, 9,400, and 9,100 ^{14}C yr BP. When converted to

calendar years, these events are dated at 11,000, 10,700, 10,400, and 10,000 cal yr BP (Table 4; Aharon, pers. comm.). Three of these discharge events correspond with the Preboreal events (PBE1-4) observed in the Petén Itzá density and $\delta^{18}O$ records (Fig. 8), as well as variations in Cariaco Ti (Fig. 11B). This may suggest that episodic meltwater discharge into the Gulf of Mexico during the Preboreal was sufficient to cause regional changes in E/P. Alternatively, the correlation between Caribbean drying and meltwater pulses to the Gulf of Mexico may represent responses to a common forcing, such as deglaciation in high northern latitudes.

Finally, we compared the Lake Petén Itzá $\delta^{18}O$ and density records with paleoclimate changes in the high-latitude North Atlantic. Bond *et al*. (2001) used fluctuations in hematite stained grains (HSG) to infer increases in drift ice associated with cool SST in the North Atlantic for the last glaciation and Holocene. From 11,500 to 8,000 cal yr BP, they recognized four distinct peaks in HSG abundance centered at 11,300, 10,300, 9,400, and 8,400 cal yr BP (Fig. 12). The three older events correlate with inferred dry climate conditions observed in the Petén Itzá $\delta^{18}O$ record (Fig. 12). Furthermore, three dry events that are also observed as density increases in our record coincide with abrupt decreases in $\delta^{18}O$ values measured in the GISP2 ice core (Fig. 13; Stuiver *et al*., 1995). The two most pronounced events, the Preboreal Oscillation (PBO) at ~11,300 cal yr BP (Björck *et al*., 1997) that corresponds to PBE1 (Table 4), and the 8.2-kyr Event (Alley *et al*., 1997) have been interpreted as periods of significant cooling in the high-latitude North Atlantic. We, therefore, suggest that cool events in the high-latitude North Atlantic were associated with dry climate conditions in the northern lowland Neotropics.

Proposed Mechanisms for Climate Change in the Preboreal and Early Holocene

Precipitation proxies in the circum-Caribbean display a coherent response during the latter part of the last deglaciation and early Holocene. This is expected because the northern

Neotropics are influenced by the same climate regime, where rainfall is related to the intensity of the annual cycle and associated displacement of the Atlantic ITCZ and Azores-Bermuda high-pressure system (Hodell *et al*., 1991; Peterson *et al*., 2000; Haug *et al*., 2001). This mechanism has been shown to operate on short (annual) to long (millennial) timescales (Hodell *et al*., 1991; Chang *et al*., 1997; Peterson *et al*., 2000; Haug *et al*., 2001; Lea *et al*., 2003; Black *et al*., 2004; Chiang *et al*., 2003, in press). In turn, the mean latitudinal position of the ITCZ and Azores-Bermuda subtropical high may be influenced by numerous factors including: tropical Atlantic SST, seasonal insolation, glacial boundary conditions, thermohaline circulation (via cross equatorial heat transport and sea ice extent), solar irradiance, and ocean-atmosphere interactions such as NAO and ENSO (Hodell *et al*., 1991; Chang *et al*., 1997; Peterson *et al*., 2000; Haug *et al*., 2001; Poore *et al*., 2003; Chiang *et al*., 2003, in press).

Long-term (glacial-to-interglacial) variations in Neotropical precipitation are affected by the seasonal distribution (Aug.-Feb.) of insolation related to variations in Earth's orbit, especially precession (Hodell *et al*., 1991; Haug *et al*., 2001). Precipitation in the northern Neotropics is enhanced when the seasonal insolation difference is high, and reduced when seasonality is low. Long-term changes in paleoprecipitation proxies (density and $\delta^{18}O$) in Lake Petén Itzá cores generally follow the signal of seasonal insolation difference at 15^{o}N (Fig .11A), but orbital forcing cannot explain the abrupt changes that occurred during the latter part of the last deglaciation and early Holocene.

During the Preboreal, the general trend toward more humid conditions in the Petén was interrupted by four dry events (PBE1-4) centered at 11,200, 10,900, 10,700, and 10,400 cal yr BP (Fig. 8). The oldest event (PBE-1) coincides with the Preboreal Oscillation (Björck *et al*., 1997; van der Plicht *et al*., 2004). The three younger events appear to correspond with episodic

diversions of glacial meltwater to the Gulf of Mexico (Table 4; Aharon, 2003) that were related to changes in glacial boundary conditions (Clark *et al*., 2001). A possible explanation for this phenomenon comes from modeling studies that impose a 6ºC cooling of the Gulf of Mexico related to the delivery of cold, fresh glacial waters to the basin (Overpeck *et al*., 1989; Oglesby *et al*., 1989; Maasch and Oglesby, 1990). These model sensitivity tests imply that cooling Gulf of Mexico SST results in a westward shift of the Azores-Bermuda high to a position over the Intra-Americas Sea. This would, in turn, suppress convection and reduce precipitation in the region (Hastenrath, 1984). Meltwater discharge during the Preboreal, however, was significantly less than that used to infer a 6ºC cooling of the entire Gulf of Mexico. Instead, meltwater fluxes were more comparable in magnitude to the largest of modern Mississippi River floods (Aharon, 2003), which probably only influenced part of the Gulf of Mexico. Alternatively, early Holocene deglacial events may have provided meltwater input to both the Gulf of Mexico and high-latitude North Atlantic, thereby causing cooling, an expansion of sea ice, and perhaps a reduction in the Atlantic meridional overturning circulation (MOC).

Two of the Preboreal Events (PBE1 and PBE4) at 11,200 and 10,400 cal yr BP, respectively, and an early Holocene event at 9,400 cal yr BP may correlate to increases in the $\delta^{18}O$ records of Lake Miragoane and Lake Valencia (Fig. 10; Curtis and Hodell, 1993; Curtis *et al*., 1999). These dry events together with another early Holocene event centered at 8,000 cal yr BP, correspond within chronological uncertainty, to cooler temperatures inferred from low $\delta^{18}O$ values in the GISP2 ice core (Fig. 13; Stuiver *et al*., 1995) and fluctuations in the abundance of hematite stained grains (HSG) found in high-latitude North Atlantic cores (Fig. 12; Bond *et al*., 2001). Bond *et al*. (2001) related fluctuations in HSG abundance with changes in the production rates of ^{10}Be and ^{14}C, such that increases in HSG abundance occurred during times of decreased

solar irradiance and cold temperatures in the high-latitude North Atlantic. Increased aridity in the circum-Caribbean may have accompanied these cooling events, and may have been caused by a southward migration of the ITCZ related to decreased solar luminosity, increased sea ice, or decreased thermohaline circulation. For example, the 8.2-kyr Event, which was the most prolonged and distinct cooling in the Northern Hemisphere since the Younger-Dryas, may have been related to both reduced solar luminosity (Muscheler *et al*., 2004) and a reduction in MOC from glacial meltwater discharge into the North Atlantic via Hudson Strait (Clark *et al*., 2001). A similar mechanism has been proposed for the Preboreal Oscillation (PBO; Björck *et al*., 1997; van der Plicht *et al*., 2004) that is equivalent to our PBE1.

Summary and Conclusions

Seismic data indicate that prior to the last deglaciation, the level of Lake Petén Itzá was about ~58 m below modern stage. This observation is consistent with previous studies of Petén lakes that indicated arid climate conditions. The last deglaciation saw an abrupt shift from arid to humid conditions in the region. The age of our oldest deep-water core from Petén Itzá is 11,250 cal yr BP, which captures only the terminal part of this arid-to-humid transition. Pollen assemblages from the base of the core demonstrate that a mesic forest had been largely established by ~11,250 cal yr BP, but Petén Itzá's level was still >35 m below modern. From 11,250 to 10,350 cal yr BP during the Preboreal Period, cores from <35 m below present water depth contain soil horizons, indicating subaerial exposure. During this period, deep-water cores from >50 m below present water depth contain gypsum sands interbedded with carbonate-rich clays, indicating several dry-wet cycles. Oxygen isotopic ratios generally decrease during the Preboreal Period indicating a trend toward more mesic conditions. This trend was interrupted,

however, by four Preboreal dry events (PBE1-4) centered at 11,200, 10,900, 10,700, and 10,400 cal yr BP. The four events correlate to decreases in the Cariaco Ti record, suggesting they may have been widespread throughout the circum-Caribbean region. Three of the events coincided with episodic diversions of glacial meltwater to the Gulf of Mexico.

At 10,350 cal yr BP, increased precipitation and lake level rise is documented in deep-water cores by cessation of gypsum deposition and the onset of lacustrine sedimentation at shallow water sites. Increased abundance of tropical mesic pollen taxa lagged this transition by ~100 yrs. This event occurred at the Preboreal-to-Boreal transition and coincided with an inferred increase in precipitation recorded throughout the circum-Caribbean. The early Holocene was a time of generally reduced climate variability and steadily increasing moisture availability except for two returns to slightly drier conditions centered at, 9,400 and 8,000 cal yr BP. The prolonged dry event at 8,000 cal yr BP correlates with inferred reductions in circum-Caribbean precipitation as well as cooler temperatures in the high-latitude North Atlantic.

Comparison of the Lake Petén Itzá record with other lacustrine and marine records from the circum-Caribbean and Gulf of Mexico suggests that climate in this region responded coherently during the Preboreal and early Holocene periods. In addition, lowland Neotropical climate during this time was tightly linked to high-latitude climate change in the North Atlantic. Although the general trend in the northern lowland Neotropics was toward increasingly mesic conditions from ~11,250 to 7,500 cal yr BP, climate became drier at times of cooling in the high-latitude North Atlantic. We speculate that the observed changes in lowland Neotropical precipitation were related to the intensity of the annual cycle and associated displacements in the mean position of the ITCZ and Azores-Bermuda subtropical high. This mechanism operated on

a variety of timescales and responded sensitively to changes in solar radiation, glacial meltwater, North Atlantic sea ice extent, and MOC.

Acknowledgements

We thank Liseth Perez, Laura Rodriguez and Jacobo Blijdenstein for field assistance, Gerard Bond for HSG and ^{10}Be data, and Paul Aharon for calibrating the LOUIS stacked-core age model, and Mike Binford for assisting with limnological data collection in 1980. We also thank Arturo Godoy and Roan McNab from the Wildlife Conservation Society (WCS), Margaret and Michael Dix from the Universidad del Valle, and the Consejo Nacional de Areas Protegidas (CONAP) for providing logistical assistance in the field. The Limnological Research Center (LRC) at the University of Minnesota supplied the coring system. Radiocarbon analyses were preformed under the auspices of the U.S. Department of Energy by the University of California Lawrence Livermore National Laboratory (contract W-7405-ENG-48). Paul Baker and Larry Peterson provided thoughtful reviews that improved the manuscript. This work was supported by National Science Foundation (NSF) grant ATM-0117148 and is a publication of the University of Florida, Land Use and Environmental Change Institute (LUECI).

References

Aharon P. 2003. Meltwater flooding events in the Gulf of Mexico revisited: implications for rapid climate changes during the last deglaciation. *Paleoceanography* **18**: DOI:10.1029/2002PA000840.

Alley RB, Mayewski PA, Sowers T, Stuiver M, Taylor KC, Clark PU. 1997. Holocene climate instability: A prominent, widespread event 8,200 yr ago. *Geology* **25**: 483-486.

Anselmetti FS, Ariztegui D, Hodell DA, Hillesheim MB, Brenner M, Gilli A, McKenzie JA. In review. Late Quaternary climate-induced lake level variations in Lake Petén Itzá, Guatemala, inferred from seismic stratigraphic analysis. *Palaeogeography, Palaeoclimatology, Palaeoecology.*

Bard E, Arnold M, Hamelin B, Tisnerat-Laborde N, Cabioch G. 1998. Radiocarbon calibration by means of mass spectrometric ^{230}Th/ ^{234}U and ^{14}C ages of corals; an updated database including samples from Barbados, Mururoa, and Tahiti. *Radiocarbon* **40**: 1085-1092.

Berger A. 1978. Long-term variations of daily insolation and Quaternary climate change. *Journal of the Atmospheric Sciences* **35**: 2362-2367.

Björck S, Rundgren M, Ingolfsson O, Funder S. 1997. The Preboreal oscillation around the Nordic Seas: terrestrial and lacustrine responses. *Journal of Quaternary Science* **12**: 455-465.

Black DE, Thunell RC, Kaplan A, Peterson LC, Tappa EJ. 2004. A 2000-year record of Caribbean and tropical North Atlantic hydrographic variability. *Paleoceanography* **19**: DOI:10.1029/2003PA000982.

Bond G, Kromer B, Beer J, Muscheler R, Evans MN, Showers W, Hoffman S, Lotti-Bond R, Hajdas I, Bonani G. 2001. Persistent solar influence on North Atlantic climate during the Holocene. *Science* **294**: 2130-2136.

Bradbury JP, Leyden BW, Salgado-Labouriau ML, Lewis Jr. WM, Schubert C, Binford MW, Frey DG, Whitehead DR, Weibezahn FH. 1981. Late Quaternary environmental history of Lake Valencia, Venezuela. *Science* **214**: 1299-1305.

Brenner M. 1994. Lakes Salpetén and Quexil, Petén, Guatemala, Central America. In *Global Geological Record of Lake Basins, Volume 1*, Kelts K, Gierlowski-Kordesch E (eds). Cambridge University Press: Cambridge, UK; 377-380.

Brenner M, Curtis JH, Higuera-Gundy A, Hodell DA, Jones GA, Binford MW, Dorsey KT. 1994. Lake Miragoane, Haiti (Caribbean). In *Global Geological Record of Lake Basins, Volume 1*, Kelts K, Gierlowski-Kordesch E (eds). Cambridge University Press: Cambridge, UK; 403-405.

Chang P, Ji L, Li H. 1997. A decadal climate variation in the tropical Atlantic Ocean from thermodynamic air-sea interactions. *Nature* **385**: 518-518.

Chiang, JCH. Present-day climate variability in the tropical Atlantic: a model for paleoclimate change? In *The Hadley Circulation: Past, Present, and Future*, H. F. Diaz and R. S. Bradley (Eds.), Cambridge University Press, in press.

Chiang JCH, Biasutti M, Battisti DS. 2003. Sensitivity of the Atlantic Intertropical Convergence Zone to Last Glacial Maximum boundary conditions. *Paleoceanography* **18**: DOI:10.1029/2003PA000916.

Clark PU, Marshall SJ, Clarke GKC, Hostetler SW, Liccardi JM, Teller JT. 2001. Freshwater forcing of abrupt climate change during the last glaciation. *Science* **193**: 283-287.

Covich AP, Stuiver M. 1974. Changes in oxygen 18 as a measure of long-term fluctuations in tropical lake levels and molluscan populations. *Limnology and Oceanography* **19**: 682-691.

Covich AP. 1976. Recent changes in molluscan diversity of a large tropical lake (Lago de Petén, Guatemala). *Limnology and Oceanography* **21**: 51-59.

Curtis JH, Hodell DA. 1993. An isotopic and trace element study of ostracods from Lake Miragoane, Haiti: A 10.5 kyr record of paleosalinity and paleotemperature changes in the Caribbean. In *Climate Change in Continental Isotopic Records, Geophysical Monograph 78*, Swart PK, Lohmann KC, McKenzie J, Savin S (eds). American Geophysical Union: Washington D.C.; 135-152.

Curtis JH, Brenner M, Hodell DA, Balser RA, Islebe GA, Hoogheimstra H. 1998. A multi-proxy study of Holocene environmental change in the Maya Lowlands of Petén, Guatemala. *Journal of Paleolimnology* **19**: 139-159.

Curtis JH, Brenner M, Hodell DA. 1999. Climate change in Lake Valencia Basin, Venezuela, ~12600 yr BP to present. *The Holocene* **9**: 609-619.

Curtis JH, Brenner M, Hodell DA. 2001. Climate change in the circum-Caribbean (late Pleistocene-to-Present) and implications for regional biogeography. In *Biogeography of the West Indies*, Woods CA (ed). CRC Press: Boca Raton, FL; 35-54.

Deevey ES, Stuiver M. 1964. Distribution of natural isotopes of carbon in Linsley Pond and other New England lakes. *Limnology and Oceanography* **9**: 1-11.

Deevey ES, Brenner M, Flannery MS, Yezdani GH. 1980. Lakes Yaxha and Sacnab, Petén, Guatemala: Limnology and hydrology. *Arch. Hydrobiol.* **57**: 419-460.

Deevey ES, Brenner M, Binford MW. 1983. Paleolimnology of the Petén Lake District, Guatemala III: Late Pleistocene and Gamblian environments of the Maya area. *Hydrobiologia* **103**: 211-216.

Fontes JC, Gonfiantini R. 1967. Component isotopique au cours de l'evaporation de deux basins sahariens. *Earth and Planetary Science Letters* **3**: 258-266.

Gasse F, Techet R, Durand A, Gilbert E, Fontes JC. 1990. The arid-humid transition in the Sahara and Sahel during the last deglaciation. *Nature* **346** 141-146.

Hastenrath S. 1984. Interannual variability and the annual cycle: Mechanisms of circulation and climate in the tropical Atlantic sector. *Monthly Weather Review* **112**: 1097-1107.

Haug GH, Hughen KA, Sigman DM, Peterson LC, Röhl U. 2001. Southward migration of the Intertropical Convergence Zone through the Holocene. *Science* **293**: 1304-1308.

Higuera-Gundy A, Brenner M, Hodell DA, Curtis JH, Leyden BW, Binford MW. 1999. A 10,300 ^{14}C-year record of climate and vegetation change from Haiti. *Quaternary Research* **52**: 159-170.

Hodell DA, Curtis JH, Jones GA, Higuera-Gundy A, Brenner M, Binford MW, Dorsey KT. 1991. Reconstruction of Caribbean climate change over the past 10,500 years. *Nature* **352**: 790-793.

Hodell DA, Curtis JH, Brenner M. 1995. Possible role of climate change in the collapse of the Maya civilization. *Nature* **375**: 391-394.

Hodell DA, Brenner M, Curtis JH, Guilderson T. 2001. Solar forcing of the drought frequency in the Maya lowlands. *Science* **292**: 1367-1369.

Hodell DA, Brenner M, Curtis JH. In press. Terminal Classic drought in the Maya lowlands inferred from multiple sediment cores in Lake Chichancanab (Mexico). *Quaternary Science Reviews*.

Hughen KA, Overpeck JT, Peterson LC, Trumbore S. 1996. Rapid climate changes in the tropical Atlantic region during the last deglaciation. *Nature* **380**: 51-54.

IAEA/WMO global network of isotopes in precipitation: The GNIP Database. 2001. http://isohis.iaea.org/ [1 July 2004].

Lachniet MS, Asmerom Y, Burns SJ, Patterson WP, Polyak VJ, Seltzer GO. 2004. Tropical response to the 8200 yr B.P. cold event? Speleothem isotopes indicate a weakened early Holocene monsoon in Costa Rica. *Geology* **32**: 957-960.

Lea DW, Pak DK, Peterson LC, Hughen KA. 2003. Synchroneity of tropical and high-latitude Atlantic temperatures over the last glacial termination. *Science* **302**: 1361-1364.

Leyden BW. 1985. Late Quaternary aridity and Holocene moisture fluctuations in Lake Valencia Basin, Venezuela. *Ecology* **66**: 1279-1295.

Leyden BW, Brenner M, Hodell DA, Curtis JH. 1993. Late Pleistocene climate in the Central American lowlands. In *Climate Change in Continental Isotopic Records, Geophysical Monograph 78*, Swart PK, Lohmann KC, McKenzie J, Savin S (eds). American Geophysical Union: Washington D.C.; 165-178.

Leyden BW, Brenner M, Hodell DA, Curtis JH. 1994. Orbital and internal forcing of climate on the Yucatan Peninsula for the past ca. 36 ka. *Palaeogeography, Palaeoclimatology, Palaeoecology* **109**: 193-210.

Maasch KA, Oglesby RJ. 1990. Meltwater cooling of the Gulf of Mexico: a GCM simulation of climatic conditions at 12 ka. *Paleoceanography* **5**: 977-996.

Magaña V, Amador JA, Medina S. 1999. The midsummer drought over Mexico and Central America. *Journal of Climate* **12**: 1577–1588.

Muscheler R, Beer J, Vonmoss M. 2004. Causes and timing of the 8200 yr BP event inferred from comparison of the GRIP ^{10}Be and the tree ring Δ^{14}C record. *Quaternary Science Reviews* **23**: 2101-2111.

Oglesby RJ, Maasch KA, Saltzman B. 1989. Glacial meltwater cooling of the Gulf of Mexico: GCM implications for Holocene and present-day climates. *Climate Dynamics* **3**: 115-133.

Overpeck JT, Peterson LC, Kipp N, Imbrie J, Rind D. 1989. Climate change in the circum-North Atlantic region during the last deglaciation. *Nature* **338**: 553-557.

Paillard D, Labeyrie L, Yiou P. 1996. Macintosh program performs time-series analysis. *AGU Eos Trans.* **77**: 379.

Peterson LC, Haug GH, Hughen KA, Röhl U. 2000. Rapid changes in the hydrologic cycle of the tropical Atlantic during the Last Glacial. *Science* **290**: 1947-1951.

Poore RZ, Dowsett HJ, Verardo S, Quinn TM. 2003. Millennial- to century-scale variability in the Gulf of Mexico Holocene climate records. *Paleoceanography* **18**: DOI:10.1029/2002PA000868.

Rozanski K, Araguá- Araguá L, Gonfiantini R. 1993. Isotopic patterns of modern global precipitation. In *Climate Change in Continental Isotopic Records, Geophysical Monograph 78*, Swart PK, Lohmann KC, McKenzie J, Savin S (eds). American Geophysical Union: Washington D.C.; 1-36.

Schmidt MW, Spero HJ, Lea DW. 2004. Links between salinity variation in the Caribbean and North Atlantic thermohaline circulation. *Nature* **428**: 160-163.

Socki RA, Karlsson HR, Gibson EK. 1992. Extraction technique for determination of oxygen-18 in water using preevacuated glass vials. *Analytical Chemistry* **64**: 829-831.

Stuiver M, Reimer PJ. 1993. Extended ^{14}C data base and revised Calib 3.0 ^{14}C age calibration program. *Radiocarbon* **35**: 35-65.

Stuiver M, Grootes PM, Braziunas TF. 1995. The GISP2 $\delta^{18}O$ climate record of the past 16,500 years and the role of the sun, ocean, and volcanoes. *Quaternary Research* **44**: 341-354.

Stuiver M, Reimer PJ, Bard E, Beck JW, Burr GS, Hughen KA, Kromer B, McCormac G, van der Plicht J, Spurk M. 1998. INTCAL98 radiocarbon age calibration, 24,000-0 cal BP. *Radiocarbon* **40**: 1041-1083.

van der Plicht J, van Geel B, Bohncke SJP, Bos JAA, Blaauw M, Speranza AOM, Muscheler R, Björck S. 2004. The Preboreal climate reversal and a subsequent solar-forced climate shift. *Journal of Quaternary Science* **19**: 263-269.

Vinson GL. 1962. Upper Cretaceous and Tertiary stratigraphy of Guatemala. *Bulletin of the American Association of Petroleum Geologists* **46**: 425-456.

Waliser DE, Shi Z, Lanzante JR, Oort AH. 1999. The Hadley Cell circulation: assessing NCEP/NCAR reanalysis and sparse in-situ estimates. *Climate Dynamics* **15**: 719-735.

Table 1 Mean ion concentrations (n = 24) and oxygen isotopic composition ($\delta^{18}O_{lw}$) of Petén Itzá lakewater (n = 34) from samples collected at various sites and water depths in June and August 2002. Oxygen isotopic composition of precipitation ($\delta^{18}O_p$) interpolated from circum-Caribbean stations in the GNIP database (IAEA, 2001). $\delta^{18}O_{lw}$ was measured on a VG Prism II mass spectrometer using a modified method from Socki *et al*. (1992). Ion concentrations were measured on a Dionex Model DX 500 chromatograph. Bicarbonate was calculated as the sum of the cation charges minus the sum of chloride and sulfate charges.

Ca^{2+}	3.15 meq l^{-1}
Mg^{2+}	1.86 meq l^{-1}
Na^{+}	0.60 meq l^{-1}
Cl^{-}	0.26 meq l^{-1}
SO_4^{2-}	2.11 meq l^{-1}
HCO_3^{-}	3.24 meq l^{-1}
Total	11.22 meq l^{-1}

$\delta^{18}O_{lw}$	+2.9‰ (VSMOW)
$\delta^{18}O_p$	- 4.0‰ (VSMOW)

Table 2 Length, water depth, and location of cores retrieved along seismic line 11 in Lake Petén Itzá in June 2002. Cores are labeled by abbreviated lake name, day-month-year, and site.

Core	Length (cm)	Depth (m)	Latitude	Longitude
PI 8-VI-02 11A	558	58.2	17.000ºN	89.779ºW
PI 5-VI-02 11B	515	51.6	16.998ºN	89.779ºW
PI 9-VI-02 11C	275	30.0	16.991ºN	89.780ºW
PI 6-VI-02 11D	210	20.9	16.988ºN	89.779ºW
PI 8-VI-02 11E	255	9.7	16.984ºN	89.779ºW
PI 9-VI-02 11F	585	63.2	17.004ºN	89.780ºW

Table 3 Accelerator Mass Spectrometry (AMS) radiocarbon dates and calibrated ages of terrestrial organic and shell material from Lake Petén Itzá Cores 11A, 11B, 11C, 11D, and 11E. All Radiocarbon ages were corrected to $\delta^{13}C$ values of –25‰, except leaf and wood samples (indicated with #), that were too small for $\delta^{13}C$ analysis and are assumed to be –25‰.

Core	Sample Type	Depth (cm)	CAMS Number	$\delta^{13}C$ (‰)	Radiocarbon Age (1σ, ^{14}C yr BP)	Calibrated Age (2σ, cal yr BP)
PI 8-VI-02 11A	Leaf	75.5	99102	-23.31	1660 ± 40	1570 ± 60
	Wood	190.5	99103	#	2095 ± 35	2070 ± 80
	Wood	247.5	101228	#	2530 ± 60	2600 ± 150
	Wood	297.5	99104	-22.27	2570 ± 45	2740 ± 35
	Wood	353.5	92837	-30.30	3240 ± 30	3435 ± 55
	Wood	369.5	99105	-31.68	3525 ± 25	3795 ± 75
	Wood	446.5	101229	-23.63	6160 ± 70	7065 ± 180
	Leaf	448.0	101230	#	6155 ± 50	7025 ± 135
	Wood	463.5	99106	#	6585 ± 35	7470 ± 40
	Wood	489.5	92836	-30.80	7925 ± 30	8720 ± 90
	Wood	504.5	101231	-28.67	8425 ± 30	9475 ± 55
	Wood	547.0	101232	#	9470 ± 110	10820 ± 340
	Wood	552.0	101233	-22.70	9555 ± 30	11015 ± 75
PI 5-VI-02 11B	Shell	280.0	94597	-2.69	3970 ± 40	4440 ± 90[a]
	Charcoal	365.0	94606	-27.12	5930 ± 40	6730 ± 70
	Wood	433.0	92835	-28.30	7330 ± 40	8105 ± 85
PI 9-VI-02 11C	Charcoal	140.0	94607	-15.67	9665 ± 45	11120 ± 60
	Shell	140.0	94598	0.47	13810 ± 45	16580 ± 480[a]
	Shell	270.0	94599	-0.56	32420 ± 290	37635 ± 315[a,b]
PI 6-VI-02 11D	Charcoal	75.0	94608	-17.92	9460 ± 45	10670 ± 110
	Shell	75.0	94600	-1.50	11025 ± 40	13020 ± 150[a]
	Shell	140.0	94601	-1.85	19320 ± 70	22950 ± 730[a]
	Shell	205.0	94602	1.59	22110 ± 90	26035 ± 105[a,b]
PI 8-VI-02 11E	Charcoal	165.0	94609	-12.71	9055 ± 50	10220 ± 70
	Shell	165.0	94603	-3.68	10280 ± 40	12070 ± 310[a]
	Shell	250.0	94604	-3.50	17250 ± 60	20540 ± 650[a]

[a] Ages are potentially subject to hard-water-lake error (Deevey and Stuiver, 1964)

[b] Radiocarbon ages were too old for INTCAL98, therefore, ages were calibrated using the following equation from Bard *et al*. (1998); Age (cal yr BP) = -3.0126×10^{-6} (^{14}C age BP)^2 + 1.2896 (^{14}C age BP) -1005

Table 4 Chronology of Preboreal events (PBE1-4) recorded in Lake Petén Itzá Core 11A compared to periods of increased meltwater delivery (MWF-5 a,c,e,g) to the Gulf of Mexico (Aharon, 2003) and the Preboreal Oscillation (PBO, Björck *et al*., 1997). Numbers in parentheses indicate (a) times of peak aridity in the Petén, inferred from $\delta^{18}O$ of ostracods, and (b) maximum meltwater fluxes to the Gulf of Mexico.

Preboreal Events (PBE)	Interval[a] (cal kyr BP)	GOM and NA Events	Interval[b] (cal kyr BP)
		MWF-5 g	9.75-10.07 (10.0)
4	10.31-10.46 (10.4)	MWF-5 e	10.23-10.43 (10.4)
3	10.66-10.80 (10.7)	MWF-5 c	10.69-10.79 (10.7)
2	10.88-11.01 (10.9)	MWF-5 a	10.97-11.07 (11.0)
1	11.15->11.25 (11.2)	PBO	11.15-11.30

Figure Captions

Figure 1 (A) Map of the northern lowland Neotropics and Gulf of Mexico showing site locations discussed in this study: 1-Petén Lake District, northern Guatemala; 2-Cariaco Basin, offshore northern Venezuela; 3-Lake Valencia, Venezuela; 4-Lake Miragoane, Haiti; 5-Louisiana slope, northern Gulf of Mexico. (B) Map of the Petén Lake District. (C) Bathymetric map of Lake Petén Itzá with the locations of cores collected along seismic line 11 in 2002. Black dots (●) indicate cores used in this study and the black line (——) is the location of seismic line 11. Cores along other seismic lines in the northern basin are also indicated (5A, 8A, 8B, 14A). 93 refers to the location of Core PI 6-VII-93 (Curtis *et al*., 1998) taken from Petén Itzá's southern basin east of the island of Flores.

Figure 2 Water column profiles of (A) temperature (ºC), (B) dissolved oxygen (mg l^{-1}), and (C) oxygen isotopic composition ($\delta^{18}O_{lw}$, ‰) of Petén Itzá lakewater. The temperature profile and samples for $\delta^{18}O$ analysis were collected on 13 August 2002 at 17.00ºN, 89.85ºW. Dissolved oxygen is plotted for May (solid line) and August (dashed line) 1980 (unpublished data).

Figure 3 (A) High-resolution seismic image of the Line 11 showing the location of piston Cores 11A-11F (see also Table 2). Note the Late Glacial/Holocene (LG/H) sequence boundary (bold dashed-solid line) and the paleoshoreline feature at ~58 m paleo water depth. (B) Images of piston cores taken along a depth transect on seismic line 11. Water depths are relative to modern (2001) lake level. Dated horizons are indicated by arrows and inter-core correlations are marked by solid lines. The LG/H boundary (bold line) is marked by dark paleosols in shallow-water Cores 11C, 11D, and 11E and gypsum precipitation in deeper-water Cores 11A and 11B.

Figure 4 Calibrated age versus depth for Lake Petén Itzá Core 11A. Core chronology was established by linear interpolation between thirteen calibrated radiocarbon dates measured on terrestrial wood and leaf samples. Average sedimentation rates vary between ~0.2 and ~0.025 cm yr^{-1}, with a transition in sedimentation rate occurring at ~3,000 cal yr BP. Dating error (2σ) on all samples is smaller than the plot symbols, except where indicated by error bar.

Figure 5 Sediment variables measured in Lake Petén Itzá Core 11D. (A) Weight percent calcium carbonate ($CaCO_3$, %), (B) weight percent organic matter (OM, %), (C) GRA bulk density (g cc^{-1}), (D) magnetic susceptibility (cgs), (E) red color intensity (nm). The dashed line (---) denotes the dated lithologic transition from a paleosol to lacustrine deposition. The thickness of the paleosol is highlighted in gray.

Figure 6 Sediment variables measured in Lake Petén Itzá Core 11A. (A) Weight percent calcium carbonate ($CaCO_3$, %), (B) weight percent organic matter (OM, %), (C) weight percent sulfur (S, %), (D) GRA bulk density (g cc^{-1}), (E) oxygen isotopic composition ($\delta^{18}O$, ‰) of ostracods. Distinct changes in sediment composition are highlighted in gray.

Figure 7 Pollen percentage diagrams from Lake Petén Itzá (A) shallow-water Core 11D and (B) deep-water Core 11B. For both cores, certain taxa (i.e. ferns, algae, aquatic vegetation, and unidentifiable pollen) were excluded from the pollen sum used to calculate percentages. Aquatic taxa were excluded so that the pollen sum reflects only terrestrial taxa. In addition, Brosimum-

type was excluded from the pollen sum of Core 11B, in order to enhance the changes in the other taxa. Excluded taxa shown in the diagrams have percentages calculated using the restricted sum as their percentages have interpretative value. Stippled curves in Core 11D represent a factor of five exaggeration of the original pollen percentages.

Figure 8 Comparison of the first-derivative of the detrended oxygen isotopic signal $d(\delta^{18}O)/dt$ of ostracods from Petén Itzá Core 11A (—◆—) with (A) density (g cc^{-1}) and (B) percent carbonate ($CaCO_3$, %). PBE1-4 designate dry events listed in Table 4 and are highlighted in gray.

Figure 9 Hypsographic curve of cumulative lake volume versus water depth. Arrows indicate inferred lake levels based on flood surface ages.

Figure 10 Oxygen isotopic ($\delta^{18}O$) records of ostracods from three circum-Caribbean lakes. (A) Lake Miragoane, Haiti, $\delta^{18}O$ (‰, 5-pt running average) of *Candona* sp. (Curtis and Hodell, 1993), (B), Lake Petén Itzá, $\delta^{18}O$ (‰, 3-pt running average) of *Limnocythere* sp., and (C) Lake Valencia, Venezuela, $\delta^{18}O$ (‰, 5-pt running average) of *Heterocypris* sp. (Curtis *et al*., 1999). Radiocarbon dates (^{14}C yrs BP) from Lakes Miragoane are based on carbonate microfossils (ostracods) that are susceptible to hard-water-lake error (Deevey and Stuiver, 1964), whereas the Lakes Valencia and Petén Itzá chronologies are based on terrestrial organic matter. Lakes Miragoane and Valencia were calibrated to calendar years, by the authors, in order to compare it with the Petén Itzá record. Each proxy is plotted on its own respective timescale.

Figure 11 (A) Comparison of density in Petén Itzá Core 11A (black line; g cc^{-1}; inverted scale) and the three-point running average of percent Titanium (gray line; Ti, %) from the Cariaco Basin (Haug *et al*., 2001), with August minus February insolation (dashed line; W m^{-2}) at 15ºN latitude (Berger, 1978). Major cooling events observed in the North Atlantic such as the 8.2-kyr Event (Alley *et al*., 1997) and Preboreal Oscillation (PBO) at ~11,300 cal yr BP (Björck *et al*., 1997) are highlighted. Major climate intervals are denoted as the Holocene (H), Preboreal (PB), Younger-Dryas (Y-D), and Bølling-Allerød (B-A). Each record is plotted on its own respective timescale. Comparisons were not made younger than 3,000 cal yr BP because human disturbance of the watershed began at this time. (B) Petén Itzá Core 11A density smoothed with a 5-pt running average and Cariaco Ti smoothed with a 15-pt running average to mute short-term variability. The Cariaco Ti record was shifted 100 yrs younger by correlating the PB/H transition. This was done to better illustrate changes observed in the two records.

Figure 12 (A) ^{10}Be Flux (10^5 atoms cm^{-2} yr^{-1}, smoothed and detrended) from the GISP2 and GRIP ice core records, after Bond *et al*. (2001), (B) stacked plot of percent hematite stained grains from North Atlantic cores (HSG, %; Bond *et al*., 2001), and (C) oxygen isotopic composition ($\delta^{18}O$, ‰) of Petén Itzá ostracods, which was smoothed with a 3-pt running average to better illustrate long-term trends. Each record is plotted on its own respective timescale.

Figure 13 Comparison of (A) Oxygen isotopic composition ($\delta^{18}O$, ‰) of ice from the GISP2 ice core (Stuiver *et al*., 1995) with (B) density (g cc^{-1}) from Lake Petén Itzá Core 11A. Major cooling events observed in the North Atlantic such as the 8.2-kyr Event (Alley *et al*., 1997) and Preboreal Oscillation (PBO) at ~11,300 cal yr BP (Björck *et al*., 1997) are highlighted. Each proxy is plotted on its own respective timescale.

Figure 1

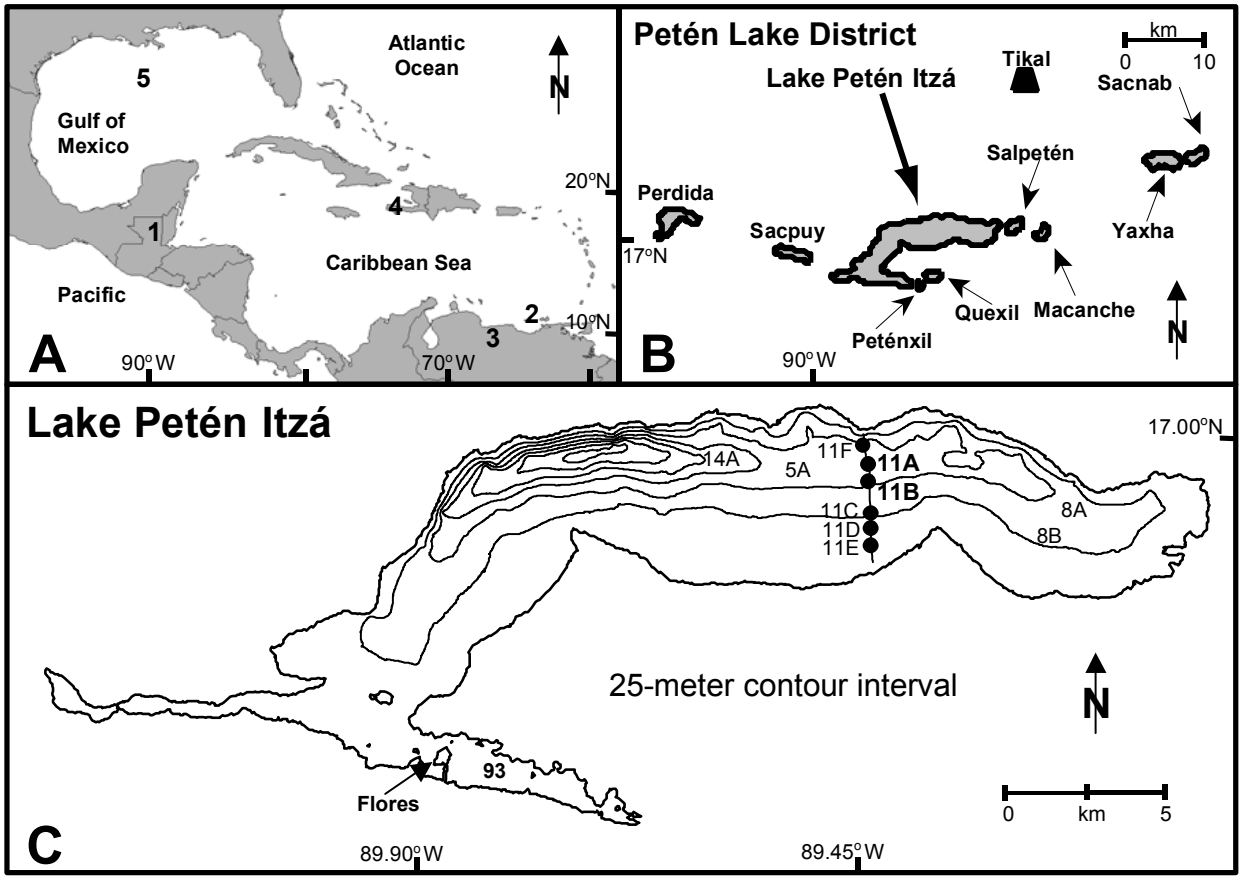
A
Atlantic Ocean
Gulf of Mexico
Pacific
Caribbean Sea
5
1
4
2
3
N
20°N
10°N
90°W
70°W
B
Petén Lake District
Lake Petén Itzá
Tikal
km
0
10
Sacnab
Salpetén
Perdida
Sacpuy
Yaxha
17°N
Quexil
Macanche
Peténxil
N
90°W
C
Lake Petén Itzá
17.00°N
14A
5A
11F
11A
11B
11C
11D
11E
8A
8B
25-meter contour interval
N
93
Flores
0
km
5
89.90°W
89.45°W

Figure 2

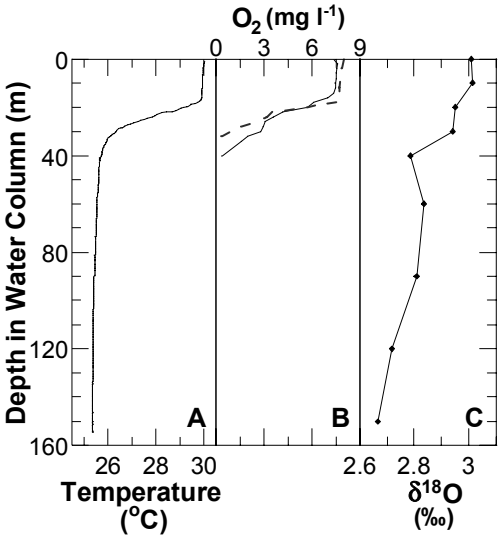
O2 (mg l-1)
0 3 6 9
0
40
80
120
160
Depth in Water Column (m)
A
B
C
26 28 30
Temperature
(°C)
2.6 2.8 3
δ18O
(‰)

Figure 3

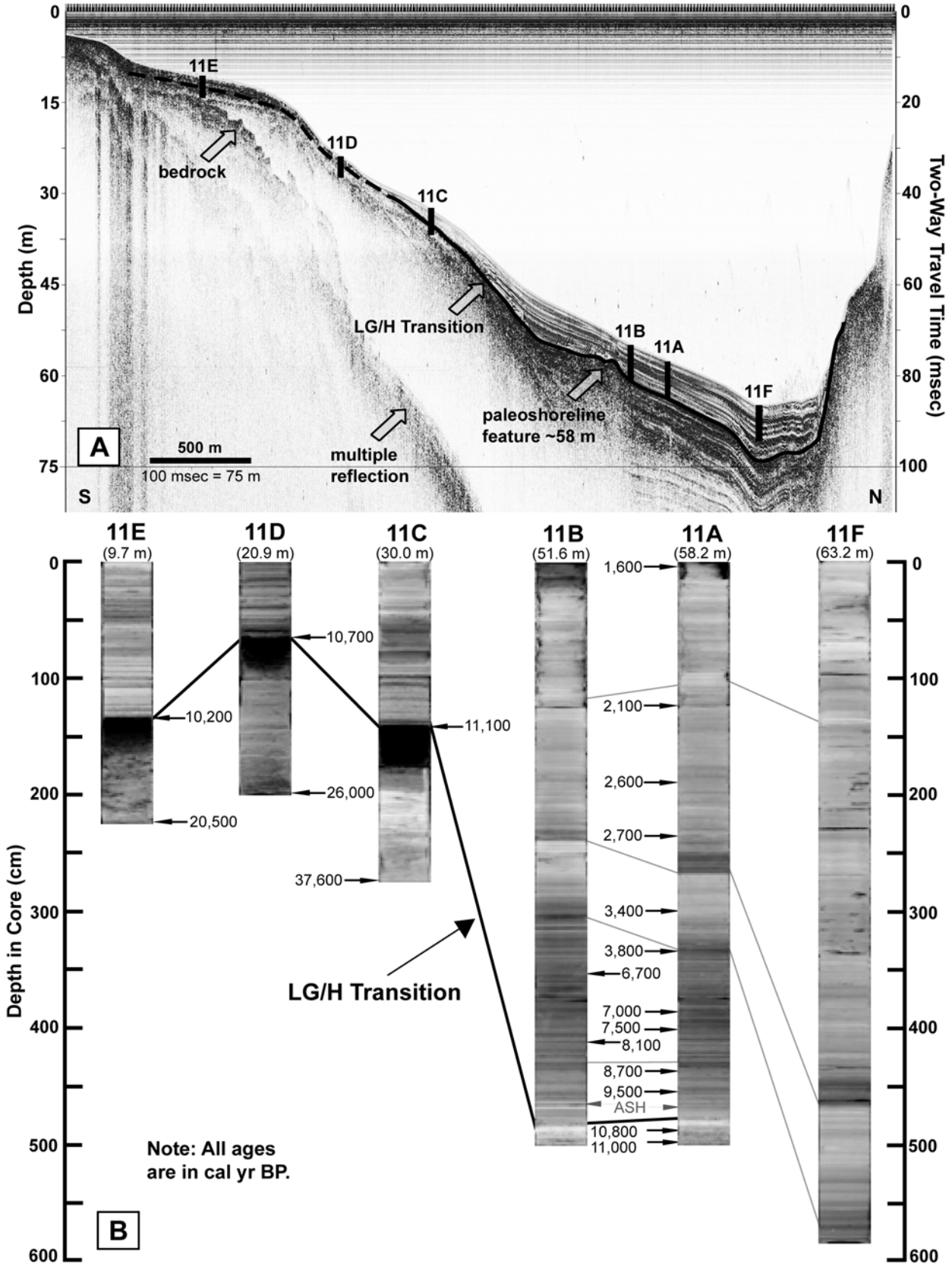
11E
11D
11C
11B
11A
11F
bedrock
LG/H Transition
paleoshoreline feature ~58 m
multiple reflection
A
500 m
100 msec = 75 m
S
N
Depth (m)
Two-Way Travel Time (msec)
0
15
30
45
60
75
20
40
60
80
100
11E (9.7 m)
11D (20.9 m)
11C (30.0 m)
11B (51.6 m)
11A (58.2 m)
11F (63.2 m)
10,200
20,500
10,700
26,000
37,600
11,100
1,600
2,100
2,600
2,700
3,400
3,800
6,700
7,000
7,500
8,100
8,700
9,500
ASH
10,800
11,000
LG/H Transition
Note: All ages are in cal yr BP.
B
Depth in Core (cm)
0
100
200
300
400
500
600

Figure 4

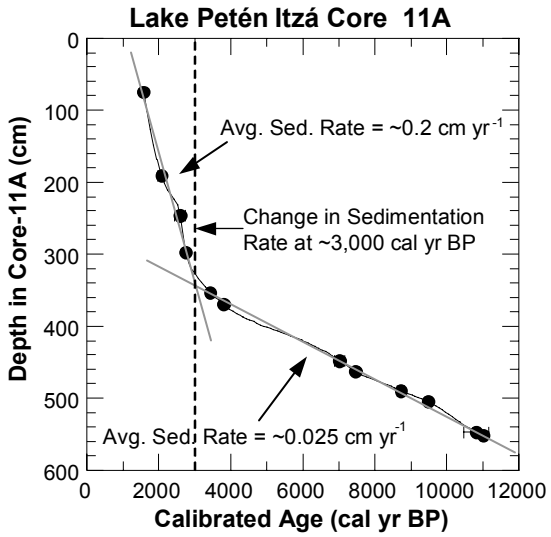
Lake Petén Itzá Core 11A
Depth in Core-11A (cm)
Calibrated Age (cal yr BP)
Avg. Sed. Rate = ~0.2 cm yr-1
Change in Sedimentation
Rate at ~3,000 cal yr BP
Avg. Sed. Rate = ~0.025 cm yr-1
0
100
200
300
400
500
600
0
2000
4000
6000
8000
10000
12000

Figure 5

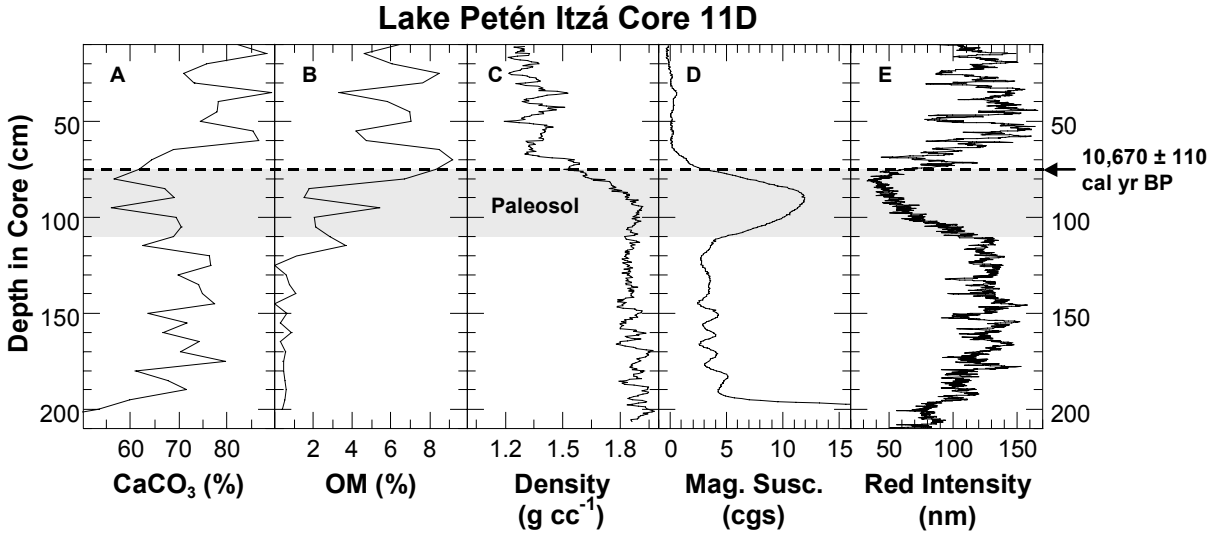
Lake Petén Itzá Core 11D
A
B
C
D
E
Depth in Core (cm)
50
100
150
200
Paleosol
10,670 ± 110
cal yr BP
60 70 80
CaCO3 (%)
2 4 6 8
OM (%)
1.2 1.5 1.8
Density
(g cc-1)
0 5 10 15
Mag. Susc.
(cgs)
50 100 150
Red Intensity
(nm)

Figure 6

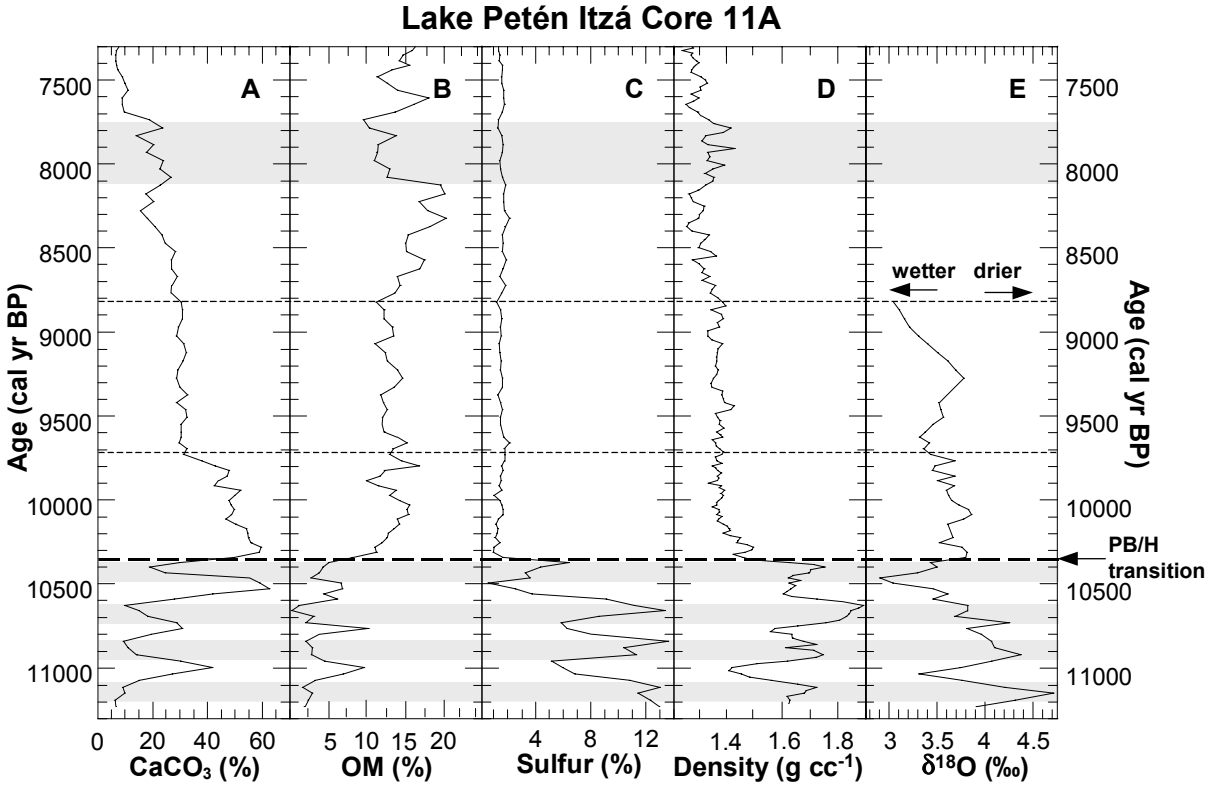
Lake Petén Itzá Core 11A
A
B
C
D
E
Age (cal yr BP)
7500
8000
8500
9000
9500
10000
10500
11000
wetter
drier
PB/H
transition
0 20 40 60
CaCO3 (%)
5 10 15 20
OM (%)
4 8 12
Sulfur (%)
1.4 1.6 1.8
Density (g cc-1)
3 3.5 4 4.5
δ18O (‰)

Figure 7

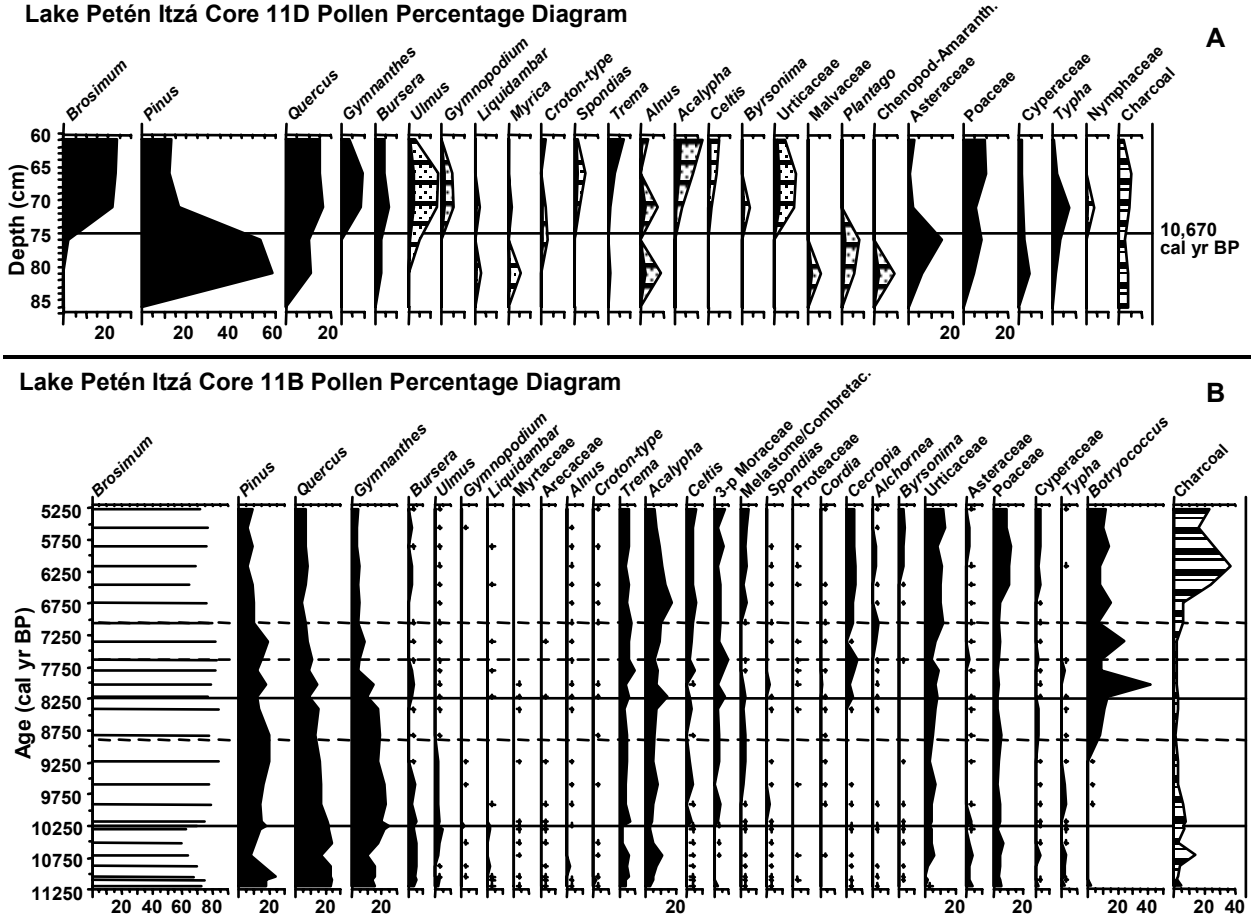
Lake Petén Itzá Core 11D Pollen Percentage Diagram
A
Brosimum
Pinus
Quercus
Gymnanthes
Bursera
Ulmus
Gymnopodium
Liquidambar
Myrica
Croton-type
Spondias
Trema
Alnus
Acalypha
Celtis
Byrsonima
Urticaceae
Malvaceae
Plantago
Chenopod-Amaranth.
Asteraceae
Poaceae
Cyperaceae
Typha
Nymphaceae
Charcoal
Depth (cm)
60
65
70
75
80
85
10,670
cal yr BP
20
20 40 60
20
20
20
Lake Petén Itzá Core 11B Pollen Percentage Diagram
B
Brosimum
Pinus
Quercus
Gymnanthes
Bursera
Ulmus
Gymnopodium
Liquidambar
Myrtaceae
Arecaceae
Alnus
Croton-type
Trema
Acalypha
Celtis
3-p Moraceae
Melastome/Combretac.
Spondias
Proteaceae
Cordia
Cecropia
Alchornea
Byrsonima
Urticaceae
Asteraceae
Poaceae
Cyperaceae
Typha
Botryococcus
Charcoal
Age (cal yr BP)
5250
5750
6250
6750
7250
7750
8250
8750
9250
9750
10250
10750
11250
20 40 60 80
20
20
20
20
20
20
20 40
20 40

Figure 8

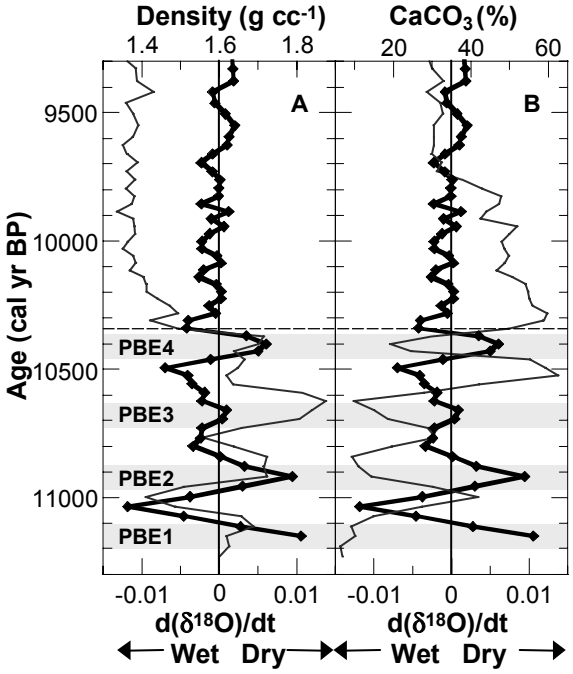
Density (g cc-1)
1.4
1.6
1.8
CaCO3 (%)
20
40
60
A
B
9500
10000
10500
11000
Age (cal yr BP)
PBE4
PBE3
PBE2
PBE1
-0.01
0
0.01
d(δ18O)/dt
Wet
Dry

Figure 9

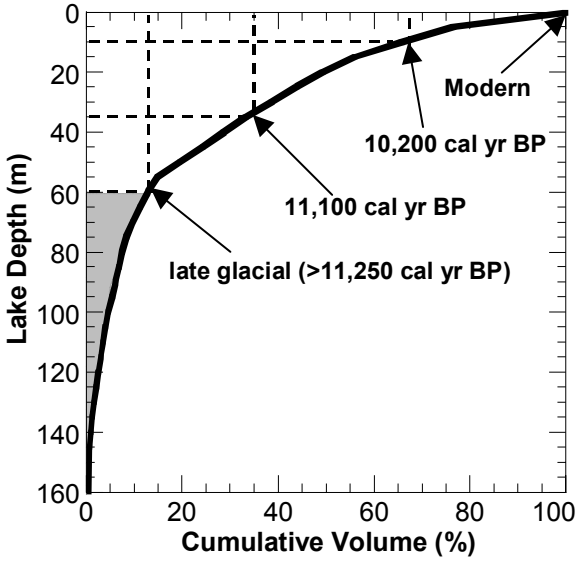
0
20
40
60
80
100
120
140
160
Lake Depth (m)
0
20
40
60
80
100
Cumulative Volume (%)
Modern
10,200 cal yr BP
11,100 cal yr BP
late glacial (>11,250 cal yr BP)

Figure 10

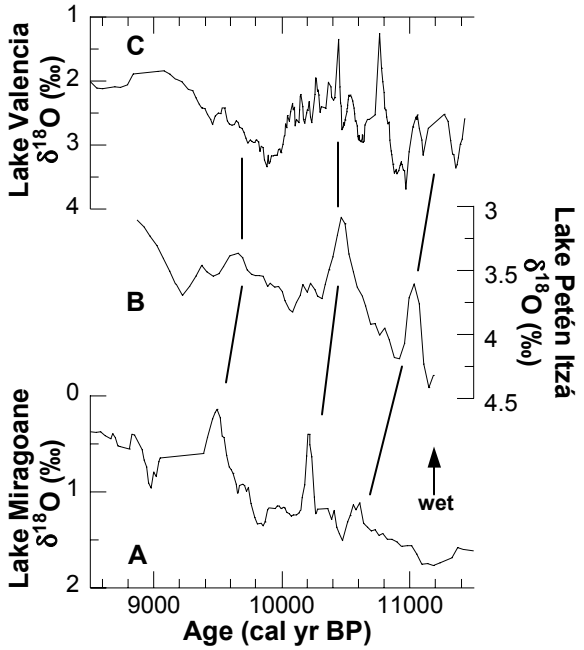
Lake Valencia
δ18O (‰)
1
2
3
4
C
B
Lake Petén Itzá
δ18O (‰)
3
3.5
4
4.5
Lake Miragoane
δ18O (‰)
0
1
2
A
wet
9000
10000
11000
Age (cal yr BP)

Figure 11

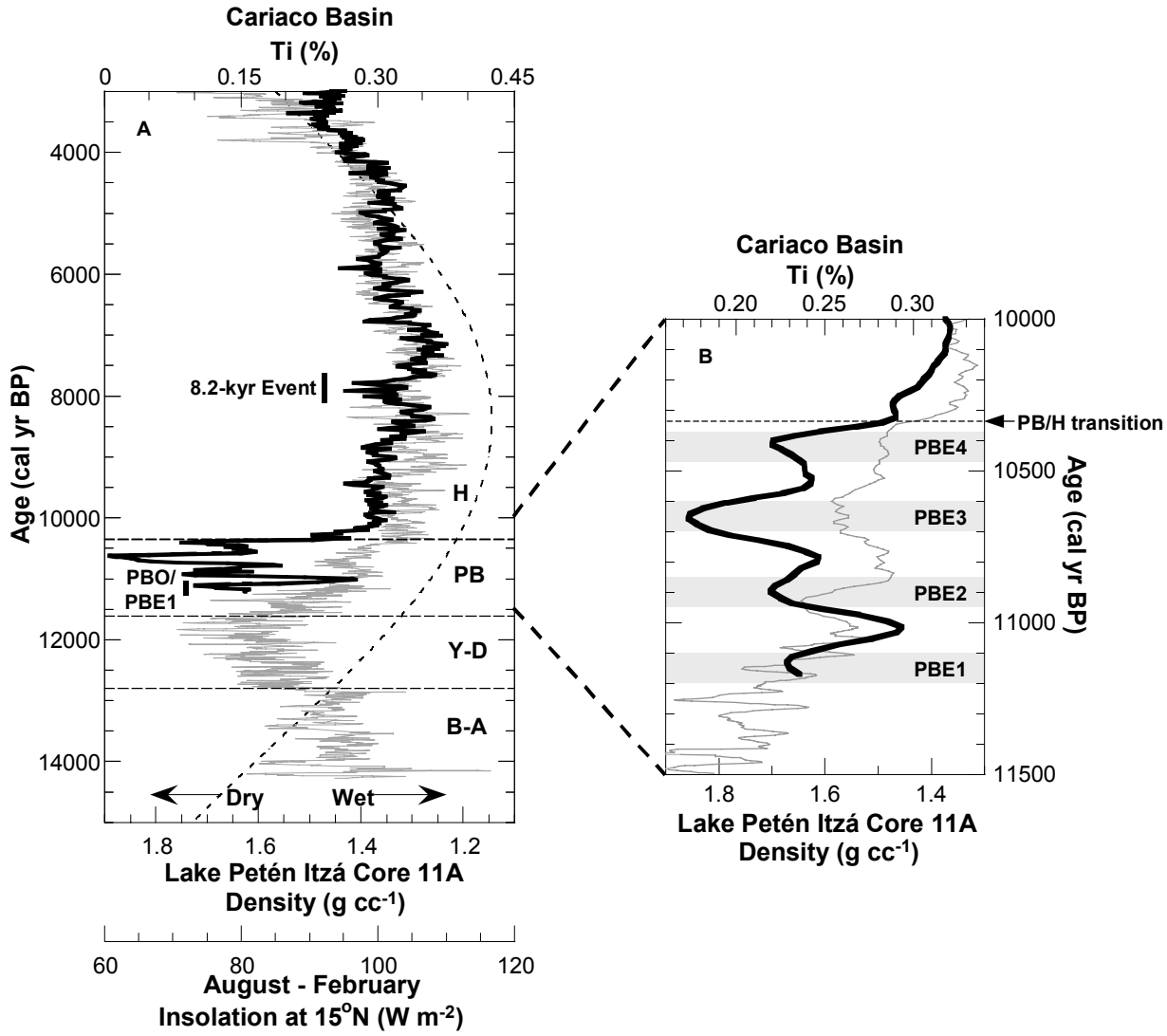
Cariaco Basin
Ti (%)
0
0.15
0.30
0.45
A
4000
6000
8000
10000
12000
14000
Age (cal yr BP)
8.2-kyr Event
H
PB
PBO/
PBE1
Y-D
B-A
Dry
Wet
1.8
1.6
1.4
1.2
Lake Petén Itzá Core 11A
Density (g cc-1)
60
80
100
120
August - February
Insolation at 15°N (W m-2)
Cariaco Basin
Ti (%)
0.20
0.25
0.30
B
10000
10500
11000
11500
Age (cal yr BP)
PB/H transition
PBE4
PBE3
PBE2
PBE1
1.8
1.6
1.4
Lake Petén Itzá Core 11A
Density (g cc-1)

Figure 12

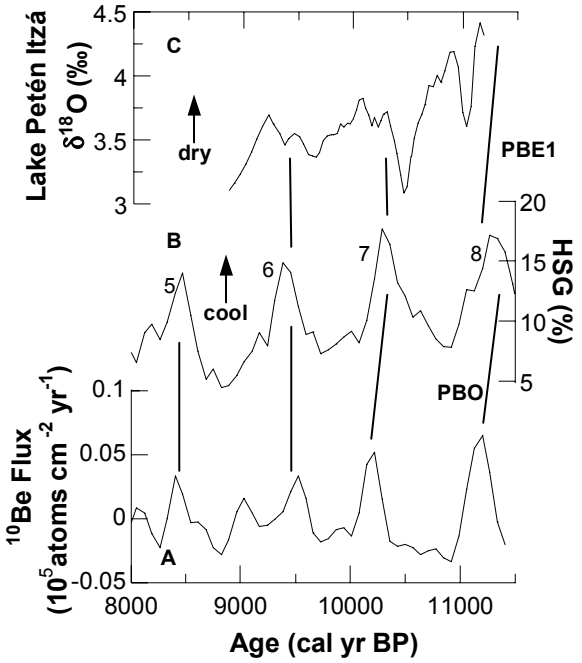
Lake Petén Itzá
δ18O (‰)
4.5
4
3.5
3
C
dry
PBE1
20
15
10
5
B
cool
5
6
7
8
HSG (%)
PBO
10Be Flux
(10^5 atoms cm^-2 yr^-1)
0.1
0.05
0
-0.05
A
8000
9000
10000
11000
Age (cal yr BP)

Figure 13

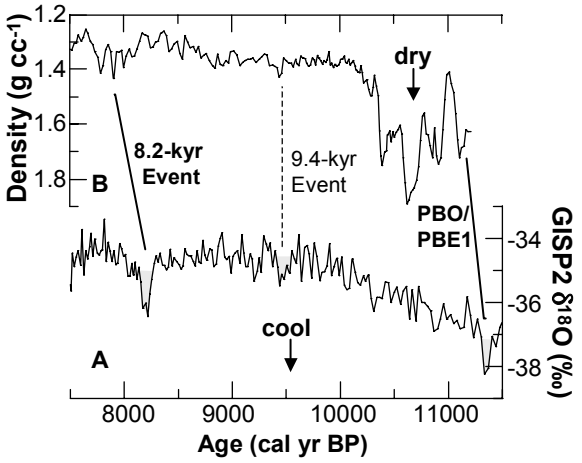
Density (g cc-1)
1.2
1.4
1.6
1.8
B
A
8.2-kyr
Event
9.4-kyr
Event
dry
cool
PBO/
PBE1
-34
-36
-38
GISP2 δ18O (‰)
8000
9000
10000
11000
Age (cal yr BP)